"Resorbable Bone Fixation Alloys, Forming, and Post-Fabrication Treatments"

Hamdy Ibrahim
PhD Candidate,
Dept. of Mechanical Industrial and
Manufacturing Engineering,
University of Toledo,
Toledo, OH 43606, USA
Hamdy.m.elsayed@gmail.com

Sajedeh Nasr Esfahani
Graduate Student,
Dept. of Mechanical Industrial and
Manufacturing Engineering,
University of Toledo,
Toledo, OH 43606, USA
nasr.sajedeh90@gmail.com

Behrang Poorganji
Senior Staff,
Yazaki Technical Center America Inc.,
3401 Calle Tecate, Camarillo, CA
93012, USA
behrang.poorganji@gmail.com

David Dean
Associate Professor,
Dept. of Plastic Surgery,
The Ohio State University,
Columbus, OH 43212, USA
David.Dean@osumc.edu

Mohammad Elahinia
Professor,
Dept. of Mechanical Industrial
and Manufacturing Engineering,
University of Toledo,
Toledo, OH 43606, USA
mohammad.elahinia@utoledo.edu

Abstract

Metallic alloys have been introduced as biodegradable metals for various biomedical applications over the last decade owing to their gradual corrosion in the body, biocompatibility and superior strength compared to biodegradable polymers. Mg alloys possess advantageous properties that make them the most extensively studied biodegradable metallic material for orthopedic applications such as their low density, modulus of elasticity, close to that of the bone, and resorbability. Early resorption (*i.e.*, less than 3 months) and relatively inadequate strength are the main challenges that hinder the use of Mg alloys for bone fixation applications. The development of resorbable Mg-based bone fixation hardware with superior mechanical and corrosion performance requires a thorough understanding of the physical and mechanical properties of Mg alloys. This paper discusses the characteristics of successful Mg-based skeletal fixation hardware and the possible ways to improve its properties using different methods such as mechanical and heat treatment processes. We also review the most recent work pertaining to Mg alloys and surface coatings. To this end, this paper covers (i) the properties and development of Mg alloys and coatings with an emphasis on the Mg-Zn-Ca-based alloys; (ii) Mg alloys fabrication techniques; and (iii) strategies toward achieving Mg-based, resorbable, skeletal fixation devices.

1. Introduction

From 2004-2005, orthopedic trauma (fractures) accounted for 72% of musculoskeletal injury charges and it was the cause of almost one-half of all the disease or injury-related hospitalizations in the United States [1, 2], similar statistics were reported in 2012 with more than $59.5 million in total hospital charges in 2011 [3, 4]. For these reported charges, intervention is necessary to reconstruct a damaged skeleton and an effective fixation hardware is needed to support surgically set bones during the healing period. Internal fixation hardware (*e.g.,* plates, screws, nails and wires) is placed over or within bones in order to hold opposing segments of fractured bone still during the healing period, without any deformation at the fracture site [5, 6]. In addition to trauma, internal fixation hardware, with or without bone grafts, is essential for skeletal reconstructive surgery [7]. While beneficial, in general, it is not practical to remove fixation hardware after the reconstructed bone has healed. However, the high stiffness of standard of care fixation hardware, relative to the stiffness of the host bone, may subsequently result in detrimental bone stress shielding and/or hardware stress concentrations [8, 9]. For children, teenagers and athletes, it is recommended to remove the hardware to avoid future bone fractures caused by unnatural loading patterns [10]. In addition, the fixation hardware may cause irritation in the adjacent soft tissue. Fixation hardware made of a biodegradable material that also offers the required stability during the healing period and subsequently degrades would mitigate stress shielding of the surrounding bone while avoiding any

potential complications associated with a second fixation removal surgery [11].

Mg alloys are the most promising biodegradable materials for orthopedic internal fixation hardware [12, 13]. The Mg alloys of interest have a low specific density (1.74-2.0) and modulus of elasticity (41-45 GPa) closer to bone (5-23 GPa for cortical bone) [14, 15]. Currently used metallic implant materials have a high modulus of elasticity (*e.g.,* 116 GPa for titanium Ti-6Al-4V) [14, 16]. The low modulus of elasticity of Mg alloys reduce the possibility of stress shielding associated with the use of stiffer metallic fixation hardware [17-19]. As a biocompatible material, Mg wires were used as a ligature for bleeding vessels more than 100 years ago [20]. As metallic fixation hardware, an Mg-based skeletal fixation plate was first used by Lambotte [21] in 1907. That work was followed by several investigations of Mg and Mg alloy bone implants. These devices studies showed promising properties in stimulating bone ingrowth and healing. Mg alloys, however, were abandoned for decades due to their undesirable degradation rate and byproducts. The fast degradation rate of pure Mg in a physiological environment results in rapid loss of mechanical integrity and genesis of hydrogen gas [22, 23]. The premature loss of mechanical integrity diminishes the fixation's function. The release of hydrogen may also be detrimental to the healing process [24]. Moreover, the strength of pure Mg and the earliest studied alloys was not high enough and much lower when compared to other biocompatible metals such as stainless steel [16, 22].

During the last decade, the development of Mg alloys useful for resorbable skeletal fixation has received greater attention as new approaches to providing

sufficient mechanical strength and useful corrosion (resorption) rates [25, 26]. Post-fabrication treatments of these alloys, such as coatings and mechanical treatments, have also been studied [27, 28]. Commercially available Mg alloys (*e.g.,* WE43, AZ91 and AZ31) despite their higher mechanical strength and enhanced corrosion resistance, are generally not considered suitable for biomedical applications due to concerns regarding their biocompatibility [29-32]. In order to achieve better biocompatibility and slower degradation, alloying with elements such as Al, Zn, Zr, Sr, Mn, Ca, and Rare earth (RE) elements (*i.e.* Gd, Y, La, Ce, Nd, Pr) has been studied [33-40]. Amongst these alloys, Mg-Zn-Ca alloys have received the greatest interest because of their excellent biocompatibility, and the possibility to tailor the mechanical and corrosion properties by changing the Zn/Ca ratio and/or heat treatments [15, 39, 41, 42].

To achieve practical Mg-based implants, it is possible to apply a protective coating to prevent the biodegradation process until a desired time point. Coating resorption rate and byproduct safety are topics of recent investigations [12, 27].

It would be a significant breakthrough if the needed fixation hardware properties and geometry can be tailored/designed to be patient-specific [1, 43]. Additive manufacturing (AM) or 3D printing of metals has received significant attention as a fabrication technique to produce highly accurate and complex-shaped structures such as patient-specific fixation hardware [44]. A number of tools can be considered for the improvement of resorbable implants' rendering. Finite element analysis (FEA) has been used in several studies to simulate and evaluate the performance of permanent fixation

hardware [45-48]. In section 3.2., we will discuss different kinds of Mg coating. Also, more in-depth discussion of additive manufacturing of Mg alloys will be the subject of section 4.5. The primary objective of this paper is to (1) present a crisp review of Mg-based alloys' design considerations for bone fixation applications based on the *in vitro* and *in vivo* performances, (2) discuss the emerging trends in the field of Mg fabrication, forming and post-fabrication treatments (e.g. coating and heat treatment) that can help to develop a Mg-based fixation hardware with enhanced biomechanical performance, (3) highlight the current challenges and strategies towards achieving Mg-based, resorbable, skeletal fixation devices.

2. Mg as a resorbable material

Bone implants have historically been made of metallic alloys such as stainless steel (316L SS), surgical grade titanium (Ti-6Al-4V) and CrCoMo due to their high strength, durability and biocompatibility [5]. The modulus of elasticity of these alloys (*e.g.,* 116 GPa for Ti-6Al-4V [16]) is significantly higher than that for bones (5-23 GPa [12]). This mismatch in stiffness leads to the phenomenon known as stress shielding. The higher stiffness of the fixation device compared to bone causes the mechanical load to transfer away from the adjacent bone [49, 50]. The absence of mechanical loading leads to a reduction in the shielded bone mass and density and subsequently a loss of bone [8]. Also, in the areas of stress concentration where the stiffer fixation develops high stresses on the bone such as around screws, a bone fracture and subsequent screws pull-out is more likely. In addition to stress shielding, leaving metallic-based fixation inside the body after the healing period, causes other problems

such as inflammatory local reactions, possible infection and the inability to adapt to bone growth near the fixation site [11, 51]. A new approach to address these issues is based on the use of biodegradable fixation. These materials should provide fixation only during the healing period and thereafter allowing the re-establishment a normal stress pattern [12]. Polymers such as polyglycolic acid (PGA), poly-L-Lactic acid (PLLA) and polycaprolactone (PCL) have been developed as biodegradable implants [38, 52-55]. Biodegradable polymers have shown excellent biocompatibility and bioresorption properties, but their lower mechanical strength results in larger dimensions, which limits their use [53, 56-58].

Mg is a resorbable material in the body. This means that the corrosion byproducts are excreted or integrated through natural metabolic processes [59]. Mg-based orthopedic fixation hardware as a biodegradable material can overcome the limitation of polymers [14]. Due to Mg alloys advantages over other metallic and polymeric-based bone implants and its resorbable nature [60], there is a driving interest in the biomaterial community to develop Mg-based bone implants [61-63]. "Velox CD ™" is a CE-approved bioresorbable Mg-based vascular closure device that was developed by Transluminal technologies [64]. Other bioresorbable Mg-based devices are currently in the final investigation stages before being available in the market for different biomedical applications such as ureteral stents [65], coronary scaffold (Biotronik Dream) [66, 67], and bone fixation hardware [68]. To date, the only commercially available Mg-based bone implant is the "MAGNEZIX ™" screw fabricated by Syntellix [69, 70]. This implant is made of uncoated Mg-Y-RE-Zr

alloy and it is approved for use in Europe for fixing small bones and bone fragments [71].

In comparison with the clinically in-use titanium-based and polymer-based fixation hardware, bone implant interface strength and osseointegration of Mg alloys have been evaluated through micro-focus computed tomography, push out force and extraction torque tests [72, 73]. Mg implants have shown increased bone-implant contact, higher implant stability and better osseointegration when compared with polymer-based and titanium-based implants especially at long implantation periods [72, 73]. Standard geometries of the currently available fixation hardware should be considered during *in vivo* evaluations since the difference in geometry may affect in the load pattern following implantation. Two such studies of Mg-based fixation hardware were conducted by Chaya *et al.* [74, 75]. They implanted plates (20 × 4.5 × 1-1.5 mm) and screws (7 mm length and 1.75 mm shaft outer diameter) made of 99.9% pure Mg in a New Zealand White rabbit ulna fracture model, as seen in Figure 1. Fracture healing and new bone formation were observed around the Mg-based fixations after 8 weeks. The hardware degraded at a rate of 0.4 ± 0.04 mm/year. After 16 weeks of implantation, bend test results showed similar flexural loads for the Mg-fixed and the healthy ulnae. An *in vivo* study in the rabbit conducted by Diekmann *et al.* [76] investigated the use of biodegradable Mg-Y-RE-Zr alloy "MAGNEZIX" interference screws for the reconstruction of the anterior cruciate ligament. Mg-based screws were implanted in the left tibiae of each of 18 rabbits for 4, 12 and 24 weeks. Maximum gas volume of 330.5 ± 83 mm^3 was detected in the medullar cavity by the 4th week. The Mg-based screws showed an average degradation rate of 0.17

mm/year over the 24 weeks of implantation. Neither inflammatory reactions nor necrosis of the tendon were observed by histological evaluation.
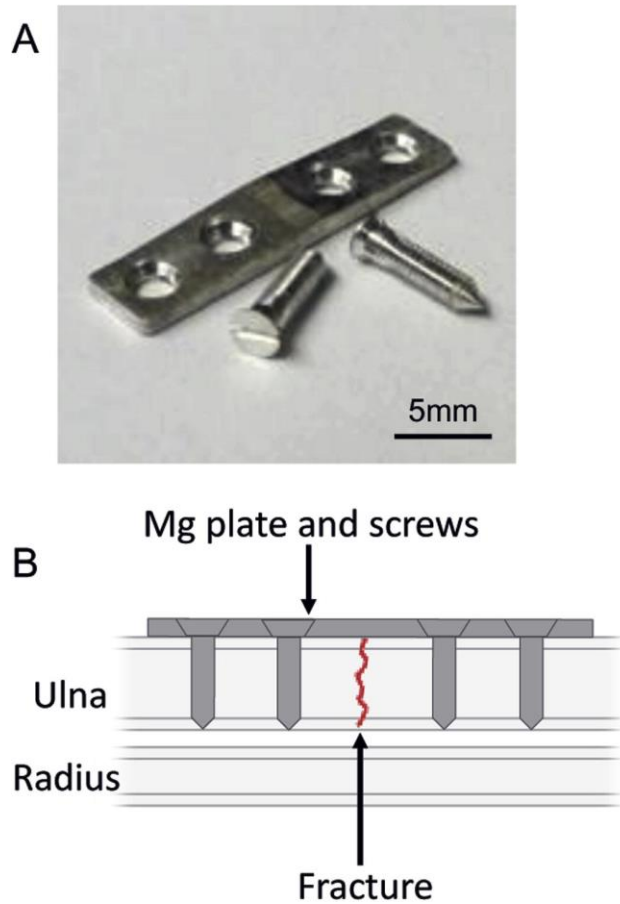

Fig. 1. Mg fixation plate and screws. Digital image showing devices prior to implantation (A). Schematic showing device placement with fractured ulna (B) (adapted from [75]).

2.1. FEA studies towards Mg-based fixation hardware

Finite element analysis can be used to calculate the state of stress and strain distribution through repaired bone and its fixation hardware. The model should include material and morphological properties of the implant, the cortical bone and the cancellous bone. Such analysis, in addition to predicting the safety of the implant, fatigue and fracture can be used to assess the possibility of bone fracture or resorption as the result of the implant [77]. This modeling approach is also used for design modification and optimization. It is desirable that the maximum Von Mises (VM) stress of cortical bone is lower than its maximum yield strength (108 MPa) for sufficient fixation hardware biomechanical stability [78, 79]. Mg-based fixation hardware should not mechanically fail while transferring compressive stress to the healing bone and should limit the interface displacement to less than 300 μm. To date, one study has been conducted by Lee *et al.* [79] to compare the Mg-based resorbable screw system in a bilateral sagittal split ramus osteotomy (BSSO) with titanium-based and polymer (Inion CPS) IN-based systems. An occlusal load of 132 N was applied to the model on the lower first molar and different fixation geometries (number of screws) were studied. Generally, Mg-based screws had a similar pattern of the VM stress distribution compared to that of titanium-based screws more than to that of IN-based screws. For example, the fixation with 5 Mg-based screws showed better biomedical stability (*i.e.*, Max. VM stress of 99.81 MPa in the cortical bone and 25.38 MPa in the cancellous bone) than the fixation with 5 IN-based screws (*i.e.*, Max. VM stress of 109.02 MPa at cortical bone and 54.72 MPa at cancellous bone) for the advancement surgery. Also for setback surgery, the maximum VM stresses developed on the cancellous bone at all fixation geometries were lowest using Mg-based screws. This study showed promising results for the use of Mg-based fixation hardware just after implantation. However, the effect of the mechanical integrity loss of these devices due to degradation on bone immobilization during the healing period has never been investigated.

2.2. The need for patient-specific fixation hardware

Conventional fixation hardware systems have been in use for many years and they usually provide satisfactory results. However, several efforts have been being attempted to replace conventional fixation hardware with custom-designed, patient-specific, fixation hardware to overcome existing shortcomings of current designs such as their unsatisfactory results in case of severe injuries and abnormal anatomy, and the possibility of postoperative complications [80, 81]. In fixation hardware, the level and the distribution of stress depends on the fracture location as well as the geometry and the material properties of the hardware [1, 43]. The stress pattern in the hardware affects the stress profile in the surrounding bone and, as a result, the morphology and density of the bone. In addition, the patient's age, gender and health status all influence bone healing. Healing time can be divided to three phases; inflammatory phase (3-7 days), the strong healing union (3-4 months), and remodeling up to a year [25]. In healthy adults, the inflammatory phase usually takes from 3 to 4 months before the bone remodeling phase starts. Bone remodeling is primarily driven by the pattern of stress. In this period, therefore, it is necessary for the bone to receive a stress profile as close as possible to that of healthy bone.

The healing time is longer for older patients [25]. Therefore, degradation time of implant should take healing time into consideration. The geometry of the implant should be designed to deliver the desired pre- and post-degradation levels of stiffness. In the beginning, the implant should be stiff enough to immobilize the bone. After the initial healing is complete, the d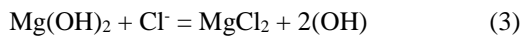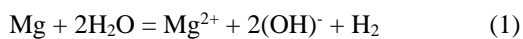egradation should result in a reduced stiffness that allows the bone to receive enough mechanical load to recreate the original loading pattern. Personalized medicine that involves a custom-designed implant system based on patient-specific anatomy and patient's case could reduce operating time and result in better treatment outcomes.

The expected excellent outcomes of using patient-specific fixation hardware are represented in the reduced complication rates, and shortened operation time and hospital stay. All these advantages will result in lower overall treatment cost. Lethaus *et al.* [82] conducted a retrospective study based on 33 patients with skull bone defects, 17 of them underwent reconstruction surgery with patient-specific implants (titanium and polyether ether ketone, PEEK) and were compared to 16 patients treated with the conventional reconstructive surgery (re-implantation of autogenous bone specimen). They found that the complication rate, rate of reoperation, hospital stay, and the total treatment cost were significantly lower for patients with the patient-specific implants (15532.08 €/patient) compared to the conventional treatment method (26086.06 €/patient).

The development of patient-specific fixation hardware has historically been limited by the available tools and the cost of fabricating the custom-designed fixation. Additive manufacturing (3D printing) has made it possible to develop the needed patient-specific fixation system. Based on individual patient data (e.g. computed tomography scan), perfectly fitting customized fixations are created [17]. More details about the additive manufacturing of Mg are discussed in section 4.5.

2.3. Corrosion of pure Mg

In addition to low yield strength (27.5 MPa) and hardness (28.9 HV) [38], Mg has a very fast corrosion rate (*e.g.,* 2.89 mm/year in NaCl solution) [13] with a corrosion potential and hydrogen evolution rate of -2.027 V [38] (- 1.906 V in another study) [42] and 56.5 mL/cm^2/day [38] respectively in simulated body fluid (SBF). In other words, Mg is highly susceptible to galvanic corrosion and its corrosion reaction in an aqueous environment (physiological environment) produces Mg ions, hydrogen (H$_2$) and hydroxyl group (OH). The hydroxyl groups quickly react with Mg ions and form a layer on the surface of magnesium hydroxide Mg(OH)$_2$ that may convert into soluble magnesium chloride (MgCl$_2$) as indicated in reactions 1 to 3 leading to an increase in the pH value [11, 83-85]. An increase in the pH (exceeding 7.8) is beneficial in slowing down the corrosion rate due to the formation of a stable magnesium hydroxide Mg(OH)$_2$ surface layer. However, such an increase in the pH value may also cause the death of tissue cells with an increase in the inflammatory response [11].

$$Mg + 2H_2O = Mg^{2+} + 2(OH)^- + H_2 \qquad (1)$$

$$Mg^{2+} + 2(OH)^- = Mg(OH)_2 \qquad (2)$$

$$Mg(OH)_2 + Cl^- = MgCl_2 + 2(OH) \qquad (3)$$

In addition, hydrogen pockets as shown in reaction 1 are formed during corrosion in the rate of 1 mL for every 1 mg of Mg. This may lead to separation of tissue and/or tissue layers, thus causing a delay in bone healing at the surgical site [24]. Also, the evolution of hydrogen may result in Mg hydrogen embitterment by the ingress of hydrogen into Mg, leading to reduction in its ductility and load bearing capacity. This reduction in ductility may cause a brittle fracture of the Mg-based fixation hardware

[11]. Corrosion of Mg has a dynamic interface between Mg surface and the body fluids and cells [25]. This dynamic interface is more emerged in the early stage of corrosion due to the change in the pH to basification, hydrogen emission and Mg and/or Ca containing corrosive surface layers [25, 86]. All these changes during the corrosion process dynamically alter the interface between Mg and the physiological environment.

2.4. Cytotoxicity and animal testing

Although the short- and long-term effects of introducing Mg and Mg alloys into the human body and their biological response on cells and tissues is not the focus of this monograph, they present an important Mg-based fixation hardware design consideration. A quick screening of the short-term biocompatibility of Mg-based alloys can be evaluated by cytotoxicity testing while animal testing may serve as a key indicator for their both short- and long-term biocompatibility. However, the *in vitro* and *in vivo* toxicity effects have not been considered in many studies during the design of Mg-based fixation hardware. This leads to uncertainty and a lack of knowledge of the effects of several alloying and coating elements when implanted especially for their long-term effects.

The biocompatibility characteristics of Mg alloying elements are different. Some elements are known to be toxic alone or alloyed with Mg such as Cd and Pb, while the biocompatibility of other elements such as Al, Sr, Li, Zr, Si and RE-elements is uncertain and has not been proven yet. Although initial studies of such elements may show low toxicity [87, 88], their long-term effects on organs or general body health are not well known. For example, the addition of 0.5 wt.% Sr to a Mg-1wt.%Ca alloy was found to have a

low overall toxicity after an *in vitro* cytotoxicity testing with a mouse osteoblastic cell line [40]. Gu *et al.* [87] evaluated the *in vitro* and *in vivo* biocompatibility of as-rolled Mg-Sr (with a Sr content ranging from 1 to 4 wt.%) as an orthopedic biodegradable alloy. The as-rolled Mg-2Sr alloy showed grade I cytotoxicity from the *in vitro* cell experiment and an enhanced mineral density and thicker cortical bone around the alloy from the intramedullary implantation test. In addition to their role in enhancing Mg mechanical properties, the addition of 1-5 wt.% Zr and 2-5 wt.% Sr to Mg was found to be biocompatible *in vitro* and *in vivo* [89]. The *in vitro* biocompatibility assessment using osteoblast-like SaOS2 cells and MTS, and haemolysis tests. A higher bone mineral density (BMD) and bone mineral content (BMC) for the Mg-Zr alloy from the *in vivo* test suggest an improved osteointegrative properties. Also, the observed increase in serum ALP activity in the implanted animals reflected bone-forming ability [89]. In another study, Gu *et al.* [88] investigated the *in vitro* biocompatibility (cytotoxicity and hemocompatibility) of nine binary Mg-1X (wt.%) alloys with different alloying elements (Al, Ag, In, Mn, Si, Sn, Y, Zn and Zr). They found that pure Mg control was the only group that did not show reduced hemolysis and adhered platelets compared to all other prepared binary alloys. Also, Mg-1Al, Mg-1Sn and Mg-1Zn were the only alloys that had no significant reduced cell viability to fibroblasts (L-929 and NIH3T3) and osteoblasts (MC3T3-E1).

On the other hand, Mg. Ca, Zn, Mn are essential nutritive elements that show no cell toxicity [41, 90]. However, they may cause toxic effects if the body intake of such elements exceeds the recommended daily dosage. The daily allowance of Mg is 0.4-0.7 g and excessive Mg in the body may lead to nausea. Also, a higher level of Mg in serum (more than 1.05 mmol/L) was found to cause muscular paralysis [16, 22, 35]. The highest daily intake that can be tolerated by the body is for Ca (0.8-1.4 g). However, inhibited intestinal adsorption of essential minerals may occur in case of excessive Ca dose [13, 91]. While, the allowable daily dose for Zn and Mn are 15-17 mg and 4 mg, respectively. Higher levels of Zn in the body may hinder bone development especially at higher concentration while excessive Mn may result in neurotoxicity [13, 22, 91]. The *in vitro* and *in vivo* biocompatibility of a binary Mg-1wt.%Ca alloy was studied by Li *et al.* [35]. No toxicity to L-929 cells was observed and the viability of cells for the Mg-1wt.%Ca alloy extraction medium was better than that of control. The *in vivo* test results showed high activity of osteocytes around the Mg-1wt.%Ca pins implanted into rabbit femoral shafts with newly formed bone at the third month. Zhang *et al.* [37] studied the *in vitro* and *in vivo* biocompatibility of a high Zn content binary Mg-6wt%Zn alloy. The hot-extruded Mg-6wt.%Zn alloy did not show any toxicity to L-929 cells. HE stained tissue (containing heart, liver, kidney and spleen tissues) and the biochemical measurements, including serum magnesium, serum creatinine (CREA), blood urea nitrogen (BUN), glutamic-pyruvic transaminase (GPT) and creatine kinase (CK) showed no harm to the vital organs and new formed bone surrounding the implanted rods into the femoral shaft of rabbits was confirmed.

As a functional way to delay the corrosion rate of Mg alloys for bone fixation applications, the assessment of the biocompatibility of a developed coating is as important as that for the coated alloy. Wang *et al.* [92] studied the *in vivo* bone response of Mg-Zn-Ca

alloy rods coated with Ca-def HA implanted into rabbit femora. Good osteoconductivity and new bone formation were confirmed by histopathological examinations. Also, Wong, *et al.* [93] studied the *in vitro* and *in vivo* biocompatibility of a AZ91 alloy coated with polymeric membrane fabricated by polycaprolactone and dichloromethane. The *in vitro* studies indicated good cytocompatibility of eGFP and SaOS-2 osteoblasts with the polymer-coated alloy, while the *in vivo* test showed lower degradation rate for the polymer-coated alloy with higher volume of new bone.

It is important to mention that the release of elements and metal ions is related to the alloy corrosion rate in the physiological environment which leads to a change in the pH value around the implant. Any change in the pH value has a negative effect on surrounding cell viability. Hence, controlling the corrosion rate is a major priority not only to maintain the fixation hardware mechanical integrity, but also to insure biocompatibility. Also, the location of the implant plays a significant role in determining the allowable limits of released elements and corrosion products based on their local toxicity to the cells and tissues adjacent to the implant. For example, the diffusion and transfer of the released elements and corrosion products is influenced by the local blood supply, distance between tissue and the implant, and the implantation time [22].

2.5. Characteristics of successful Mg-based bone fixation hardware

In spite of the numerous advantages of Mg as a biomaterial, pure Mg cannot satisfy all the clinical requirements for internal fixation hardware due to its low mechanical properties and undesirable corrosion behavior. The required mechanical properties of Mg-based fixation hardware can be determined by combining finite element analysis (FEA) studies of the fixation procedure and static *in vitro* material testing. These studies then identify the required mechanical behavior of fixation to restore the normal stress-strain trajectories [77, 94]. Strength higher than 200 MPa, elongation higher than 10% and corrosion resistance less than 0.5 mm/year (SBF at 37ºC) have been suggested to be the desired characteristics for resorbable bone fixture [95]. Fatigue, creep, and stress relaxation are other important mechanical parameters that should be considered during the material selection and design of Mg-based fixation hardware. Also, the degradation by-products (especially hydrogen) should be guaranteed that are removed by excretion without causing any toxicity to the body cells locally and/or systemically [94, 96]. A rate of 0.02 mL/cm^2/h as a tolerated level of hydrogen evolution in the human body has been proposed [97]. To this end, suitable alloying and coating are required.

3. Mg alloying and fixation device coatings

Microstructure is the key factor that affects both mechanical and corrosion performance of Mg-based biomaterials. Microstructure can be altered by alloying (*i.e.*, changing the chemical composition) as well as mechanical or heat treatment [11]. Furthermore, alloying can reduce corrosion rate and coating the surfaces of Mg-based fixation hardware delays corrosion. In this section, we will discuss Mg alloying and fixation device coating, while mechanical and heat treatments will be covered in section 4.

9

3.1. Alloying

Solid solution strengthening, precipitate hardening and grain refinement strengthening are the main alloying mechanisms for improving the mechanical properties of Mg alloys [27]. Because of the hexagonal-closed-packed (HCP) crystal structure and the atomic diameter of Mg (0.320 nm), a wide range of elements such as Al, Zn, Ca, Zr, Si, and Rare Earth elements can form solid solutions with pure Mg [12, 13]. Numerous studies have been conducted on the feasibility of Mg alloying for orthopedic device applications by characterizing their microstructure, mechanical properties, corrosion behavior and biocompatibility using both *in vitro* and *in vivo* studies. Mg-Ca, Mg-RE, Mg-Zn and Mg-Zr are the most studied Mg-based alloying systems [14, 37, 38, 88, 98, 99]. Alloying elements have different toxicity (biocompatibility) characteristics. For example, Cd and Pb are well known to be toxic elements alone or alloyed with Mg [13]. However, Ca, Sr, Zr, Mn and Zn alone or alloyed with Mg are shown to be biocompatible [13, 35, 60]. Aluminum was initially considered but has been found to cause hepatotoxicity or allergic reactions [100, 101] with the potential of leading to Alzheimer's disease [102] and it may also cause muscle fiber damage [103]. The release of RE elements (*e.g.,* yttrium) as an alloying element was found to cause severe hepatoxicity [104, 105]. Mg-Ca, Mg-Zn and Mg-Zn-Ca have been found to be the most promising alloying systems because of their superior biocompatibility, moderate strength and corrosion characteristics. We will discuss more about these alloying systems here. For more details about other Mg-based alloying systems, the reader can be referred to [12, 13]. It is important to note that the presence of impurities such as Fe, Ni, Be and Cu reduces the strength of Mg alloys while accelerating their corrosion rate [106]. Impurity levels of these elements should be kept within the physiological tolerance limit (Fe: 30–50, Ni: 20–50, Be: 2–4 and Cu: 100–300 ppm by weight) [106, 107]. Adding certain alloying elements (*e.g.,* Mn and Zn), or using the zone solidification method can eliminate the harmful effects of impurities [13].

3.1.1. Mg-Ca alloys

Mg-Ca alloys have received considerable attention for orthopedic fixation applications. They have low density (1.55 g/cm3), low cost, as well as the beneficial role of co-releasing of Mg and Ca ions during bone healing and remodeling [13]. The addition of Ca to pure Mg also protects the Mg alloy from oxidation during casting. This protection is due to the formation of a thin dense CaO film foam on the surface that could prevent ignition of Mg and reduce molten metal surface tension [108, 109]. Furthermore, the addition of Ca to Mg assists in grain refinement, strengthening the alloy over pure Mg [12]. *In vitro* and *in vivo* studies have revealed that a mixture of $Mg(OH)_2$ and hydroxyapatite was formed on the surface of Mg-Ca alloys with new formation of bone on this surface after 3 months of implantation [35]. However, the rapid degradation in the physiological environment is the main obstacle in using uncoated Mg-Ca as bone fixation hardware [14]. Generally, an Mg-Ca alloy with Ca content of less than 45 wt.% is composed of lamellar eutectic phases of α-Mg + Mg_2Ca [39, 109, 110]. The Mg_2Ca secondary phase has a high average melting temperature of 715 °C [111]. However, Li *et al.* found reduced corrosion resistance as the proportion of Mg_2Ca intermetallic compound in the alloy microstructure increases [35]. This suggests that a Ca content above the solubility limit (1 wt.%) leads to

increased formation of the Mg_2Ca intermetallic compound, thus, the deterioration in the Mg-Ca alloy corrosion resistance [12, 35]. In other words, only the Mg-1wt.%Ca alloy has no toxicity and degrades gradually enough to allow bone to heal fixated. Total absorption took place after 3 months of implantation in rabbit femoral shafts.

3.1.2. Mg-Zn alloys

Zinc is less corrosive than Mg and is known to support the immune system. It is also involved in various aspects of cellular metabolism [37, 91]. From a material viewpoint, the addition of Zn to pure Mg is known to improve strength due to the formation of the MgZn intermetallic compound and refining (reducing) the grain size [109, 112]. Also, the presence of Zn in Mg alloys mitigates the adverse corrosion effect of impurities such as Fe and Ni [38]. Koç et al. [113] studied the influence of content up to 3 wt. % on the mechanical and corrosion properties of the as-cast binary Mg-Zn alloy. Mechanical properties and corrosion resistance were found to increase by increasing the content of Zn% in the prepared Mg-Zn alloys. ZK30 and ZK60 are two examples of commercial Mg-Zn based alloys with a Zn content of less than 5.5 wt.%. For example, the chemical composition of ZK30 is Mg-3wt.%Zn-0.6wt.%Zr-0.007wt.%Fe. Zhang *et al.* [37] investigated a solution-treated and hot-extruded Mg-6wt.%Zn alloy as a biodegradable material. The immersion test results showed that the hydroxyapatite (HA) and other Mg/Ca phosphates are the corrosion products of this alloy seen at the surface in SBF. The *in vivo* results showed that Mg-Zn implanted rods in the femoral shaft of rabbits were gradually absorbed at a rate of 2.32 mm/year without any harmful effects to vital organs.

In comparison to the Mg-rich alloys, Zn-rich Zn-Mg alloys offer lower corrosion rates and reduced hydrogen evolution [22]. The Zn-rich alloys are easier and safer to fabricate due to their lower reactivity and lower melting points [114]. Vojtěch *et al.* [114] investigated the effect of adding 1-3 wt.% Mg around the eutectic point. Zn-1wt.%Mg alloy showed the maximum yield strength and elongation of 90 MPa and 2% respectively with a corrosion rate of less than 0.145 mm/yr. This rate is significantly lower than any as-cast Mg-rich alloy. Murni *et al.* [115] evaluated the cytotoxicity of Zn-3wt.%Mg alloy through osteoblast cell-material interaction. They found that the Zn-rich alloy was not cytotoxic. The addition of low amount of Mn to Zn-1-1.5wt.%Mg alloys was found to enhance their corrosion and mechanical properties [116]. The disadvantages of Zn-Mg alloys are, the limited ductility (elongation 0.25-2%), higher density (~7.14 g/cm^3) and higher stiffness (modulus of elasticity ~108 GPa). Table 1 presents a quantitative comparison between the as-cast Mg-1wt.%Zn alloy and Zn-1wt.%Mg alloy as two examples of the Mg-rich and Zn-rich alloys, respectively.

Table 1 The physical, mechanical, corrosion and processing characteristics of the as-cast Mg-1wt.%Zn and Zn-1wt.%Mg alloys [88, 114].

Property	Mg-rich (Mg-1wt.%Zn) alloy	Zn-rich (Zn-1wt.%Mg) alloy
Relative density	~1.74	~7.14
Modulus of elasticity (GPa)	~45	~108
Yield Strength (MPa)	25.5	~90
Tensile Strength (MPa)	134	150
Elongation (e%)	18.2	~1.75
Corrosion in SBF	Fast (1.52 mm/yr)	Slow (~0.06 mm/yr)
Melting Temp. (ºC)	~650	~420

3.1.3. Mg-Zn-Ca alloys

Ternary Mg-Zn-Ca alloys have improved the biocompatibility and mechanical characteristics over pure Mg and binary Mg-Ca alloys, while lower density than Mg-Zn alloys and desirable anti-bacterial properties [117, 118]. In the Mg-rich alloy, various phases can be produced on the grain boundaries that result in different degradation and mechanical properties; the key differentiating factor to this end, is the Zn/Ca atomic ratio. The eutectic phase α-Mg+Mg_2Ca+$Ca_2Mg_6Zn_3$ form when the Zn/Ca atomic ratio is less than 1.1-1.2 [119-121] or 1.4 in another study [122]. Above these limits, in addition to the primary Mg, the lamellar eutectic phase α-Mg+$Ca_2Mg_6Zn_3$ is observed [123]. However, only one study by Zander and Zumdick [124] reported presence of the presence of emblematic amount of Mg_2Ca phase above these limits for the Mg-1.8wt.%Zn-0.6wt.%Ca alloy (Zn/Ca atomic ratio = 1.84). The presence of the $Ca_2Mg_6Zn_3$ phase has a more rapid corrosion rate with better mechanical properties, and an increased level of the corrosion byproduct brucite ($Mg(OH)_2$) and hydroxyapatite forms on the surface [35, 120]. This atomic ratio, as demonstrated by Larionova *et al.* [122], affects the interplanar distances in rapidly solidified alloys. An increased Zn/Ca atomic ratio leads to contraction of the phase lattice and a decreased value causes phase lattice expansion.

The high loading of alloying elements in binary systems (*e.g.,* Ca in the Mg-Ca) leads to an increased percentage of the precipitated intermetallic compounds (*e.g.,* Mg_2Ca) [60]. Similarly, the percentage of such compounds for the Mg-Zn-Ca ternary alloys increases at a high loading of Zn and Ca (*e.g.,* Mg_2Ca, $Ca_2Mg_6Zn_3$, MgZn and $MgZn_2$). An increased percentage of these intermetallic compounds results in higher strength accompanied by more rapid corrosion rates. Ca content of less than 0.5 wt.% was found as the optimum percentage for grain refinement of the Mg-rich Mg-Zn-Ca-Mn alloys [121]. It was also reported that the addition of more than 1 wt.% Zn to the Mg-0.5wt.%Ca and the Mg-1wt.%Ca alloys significantly improves corrosion resistance [120, 125, 126]. However, a higher Zn loading above 2 to 3 wt.% causes a reduction in the corrosion resistance with significant deterioration above 5 wt.% [41, 60, 120, 125].

3.1.4. Mg-Zn-Ca bulk metallic glasses (BMGs)

Mg-Zn-Ca bulk metallic glasses (BMGs) have been studied as an alternative biodegradable fixation material with superior strength and corrosion resistance in comparison with traditional cast Mg-Zn-Ca alloys [118, 127]. Unlike the crystalline atomic structure of cast alloys, Mg-Zn-Ca glasses have disordered atomic (glass-like) structure [128]. The amorphous glassy structure is usually a result of a rapid cooling process where the molten alloy crystalline phases do not have enough time to nucleate and grow, as a results, the materials undergoes a glass transition and freeze in an amorphous glassy state [128, 129]. *In vivo* pig study conducted by Zberg *et al.* [128] indicated good tissue compatibility with wound-healing process signs and less hydrogen evolution for the amorphous Mg-Zn-Ca BMG than the crystalline alloy. The cast rods were melt-spun into glassy ribbons of approximately 50 µm thickness in a helium atmosphere. Subsequently, a copper mold injection casting system was used to produce 0.5 mm thick Mg-Zn-Ca BMG samples in an argon atmosphere. The glassy (60+x)Mg-(35-x)Zn-(5)Ca alloy was found to be the most promising Mg-Zn-Ca BMG with a range of tensile strength from 675 to 894 MPa

and an elastic range of less than 4 percent. The main limitations of Mg-Zn-Ca BMGs are the limited processing time available before the onset of crystallization, small critical casting thickness of approximately 3 mm, and the poor formability [118, 128, 130]. These limitations result in a difficulty in creating fixation devices of Mg-Zn-Ca BMGs.

3.1.5. Quaternary Mg-Zn-Ca-X alloys

To further tune the properties of the Mg-based biocompatible and resorbable alloys for bone fixation devices, a limited number of elements such as Mn and Zr can be added to Mg-Zn-Ca alloys. These alloying elements improve properties by incorporating essentially insoluble metallic impurities such as Fe and Ni into harmless intermetallic phases (*e.g.,* AlMnFe phase in Mg-Al alloys) [12, 131]. In several studies, Mn (up to 1 wt.%) was added to different binary and ternary Mg alloys to enhance corrosion resistance. Bakhsheshi-Rad *et al.* [38] studied the mechanical and corrosion properties of various binary Mg-Ca and quaternary Mg-Ca-Zn-Mn alloying systems. They found that the addition of 0.5 wt.% Mn to the Mg-2wt.%Ca-2wt.%Zn and the Mg-2wt.%Ca-4wt.%Zn alloys enhances the mechanical properties and the corrosion resistance by decreasing the grain size to 78 μm and 59 μm, respectively. The small grain size provides a smoother surface, thus, fewer surface pits are present than in both Mg-Ca and Mg-Ca-Zn alloys. Also, it was found that the quaternary Mg-Ca-Zn-Mn alloys have reduced corrosion by the formation of a brucite ($Mg(OH)_2$) protection than the other studied alloys. It has been shown that these quaternary alloys with 2 wt.% Zn have better mechanical and corrosion performance than those with 4 wt.% Zn.

The addition of Zr to Mg-Zn-Ca alloys improves corrosion resistance. This effect is observed at Zr content of less than 0.42 wt.%. Higher concentrations of Zr, while improving strength due to grain refining, speeds corrosion [12, 60]. Qu *et al.* [132] developed a quaternary Mg-Zn-Ca-Y alloy for bone fixation. In their study, the alloy with Mg–2.0wt.%Zn–0.5wt.%Ca–1.0wt.%Y chemical composition was implanted in rabbits to study biocompatibility for different durations (until 24 weeks). Low levels of Lymphocytes and macrophages were observed around the local muscle tissue during the first week revealing the presence of a mild inflammatory cells. After 2-4 weeks the inflammatory cells decreased and completely disappeared after 12 weeks. Also, a thin fibrous membrane was observed around these implants after 2 weeks. The fibrous membrane's thickness (15-25 μm) remained within the U.S. ASTM-F4 implant requirements (<30 μm) for the 24-week implantation period. When compared with pure Mg, this alloy has a slower degradation rate with desirable biocompatibility. To this end, Mg-Zn-Ca alloys possess the best mechanical and corrosion properties in addition to being biocompatible. Also, the addition of Mn, Zr and/or Y to Mg-Zn-Ca alloys was found to significantly enhance the biomechanical performance. The mechanical and corrosion properties of as-cast binary, ternary and quaternary Mg-Zn-Ca alloys are listed in table 2. The values of corrosion properties vary one study to another for similar alloy chemical compositions. This can be attributed to variation in alloy microstructure during preparation and the non-strict conditions of the conducted corrosion tests within each study.

Table 2. The tensile properties and the *in vitro* electrochemical corrosion characteristics for different Mg-Ca, Mg-Zn, Mg-Zn-Ca and Mg-Zn-Ca-Mn alloys.

Alloy composition (%wt.)	Tensile properties			*In vitro* electrochemical corrosion characteristics (SBF)			Ref.
	0.2% Yield strength (MPa)	Tensile strength (MPa)	Elong. (%)	Corrosion potential E_{corr} (µv vs. SCE)	Current density i_{corr} (µA/cm²)	Calculated corrosion rate (mm/year)	
Pure Mg	27.5	97.5	7.31	-2027.4	370.7	8.47	[38]
Mg-0.5%Ca[a]	51	91	5.0	-1876	186	-	[98], [39]
Mg-2%Ca	47.2	115.2	3.05	-1996.8	301.7	6.84	[38]
Mg-4%Ca	34.5	77.4	2.10	-2054.5	395.7	9.04	[38]
Mg-1%Zn[b]	25.5	134	18.2	-1822	67.3	1.52	[88]
Mg-1%Zn[c]	80	127	16	-1830	124	-	[113]
Mg-3%Zn[c]	91	147	12	-1710	102	-	[113]
Mg-2%Zn-3%Ca	117	145	0.57	-1640 (Hank's)	3.86 (Hank's)	-	[125]
Mg-4%Zn-0.2%Ca-	60	185	12.5	-1700	267	2.05	[42]
Mg-2%Zn-2%Ca-0.5%Mn	78.3	168.5	7.83	-1616.6	78.3	1.78	[38]
Mg-2%Zn-0.5%Ca-1.2%Mn[d]	72	187	9.1	-1496	57.2	-	[121]

[a] The tensile properties were adopted from Ref. [98], while the corrosion properties were adopted from Ref. [39].

[b] The tensile properties were deduced from Fig. 2 in Ref. [88].

[c] The tensile properties were deduced from Fig. 4 in Ref. [113].

[d] The tensile properties were deduced from Fig. 5 in Ref. [121].

3.2. Coating

Coating Mg alloys improves their corrosion resistance in a physiological environment [12, 25, 133, 134]. Coating must be biocompatible and have high corrosion resistance to maintain the mechanical integrity of the fixation hardware during the initial bone healing period. Based on the interaction between the coating and the Mg alloy, coatings can be classified into three categories: substrate-involving coatings, non-substrate-involving coatings, and composite coatings [25]. Alkaline oxidation, fluoridation and micro-arc oxidation (MAO) are some examples of the substrate-involving coating techniques [25]. Gu *et al.* [135] performed an alkaline oxidation process by soaking a Mg-1.4wt.%Ca alloy in three alkaline solutions (Na_2HPO_4, Na_2CO_3 and $NaHCO_3$) for 24 h followed by annealing at 773 K for 12 h. The surface treated alloy showed an improved corrosion resistance and slower increase of the solution pH value, due to the formation of a magnesium oxide layer (MgO) of thickness of less than 26 μm. Lei *et al.* [136] employed an anodic electrodeposition process in a concentrated potassium hydroxide (KOH) solution followed by heat treatment in air. In this process, a MgO coating was produced on an Mg-5.5-6.5wt.%Zn-1.0-1.5wt.%Ca alloy, thereby slowing the corrosion rate. Mousa *et al.* [137] used an anodization process with SBF as the electrolyte to deposit a protective apatite-like coating layer, mainly composed of MgO phase, on AZ31B Mg alloy. The anodizing voltage was found to have a significant effect on the coating hardness and corrosion resistance.

Micro-arc oxidation (MAO), also referred to as, plasma electrolytic oxidation (PEO) or micro plasma oxidation (MPO), is one of the most studied coating processes due to its simplicity and the formation of a hard protective oxide layer on the surface leading to enhanced corrosion resistance. During the MAO process, a highly adherent ceramic oxide coating is formed due to partial short-term melting of the oxide layer caused by a high voltage plasma discharges [138]. One of the remarkable features of MAO coatings is the presence of pores and cracks on the coating surface. This results in higher bond strength between the coating and the Mg alloy substrate [96]. MAO coating also enhances adhesion with subsequent organic or polymeric coatings [139].

While MAO coating usually shows good protection for a few weeks, the corrosion resistance quickly degrades thereafter due to the presence of surface pores [140, 141]. To address this limitation, one possible solution is controlling the process parameters and the electrolyte to change the distribution and interconnectivity of the pores [142-144]. For example, fine pores with better corrosion resistance are produced at lower voltages [145]. It is also possible to seal the outer layer pores and cracks with additional layers of ceramic coatings (*e.g.,* hydroxyapatite [HA]) and/or polymeric coatings [96, 146]. Other solutions include the pretreatments using cerium conversion coating or increasing the thickness of the barrier layer [96, 147, 148].

Calcium phosphate (Ca/P) coatings such as hydroxyapatite (HA) and tricalcium phosphate (TCP) have been used in bone implants to improve the biocompatibility and biological response (bone ingrowth) as a non-substrate-involving coating. These ceramic coatings also offer a biocompatible platform for controlled drugs elution during the corrosion process such as antibiotics. The crystalline

hydroxyapatite (HA), which is the most stable Ca/P compound in the human body, has been extensively studied as a promising Mg alloy coating [12]. Wang *et al.* [92] studied the effect of calcium-deficient hydroxyapatite (Ca-def HA) coating on the degradation behavior and bone response of a Mg-1wt.%Ca-1wt.%Zn alloy. The samples were coated using a pulse electrodeposition process. The coated Mg alloys had a significantly slower *in vivo* corrosion rate (0.15 mm/year) compared to the uncoated samples (0.8 mm/year). Wang *et al.* [149] used a similar approach and showed superior corrosion resistance and loss of mechanical properties in the coated samples. In a slow strain rate test in SBF with extension rate of 2.16×10^{-5} mm/s until fracture, Ca-def HA coated samples had a higher ultimate strength of 152 MPa than that of the uncoated samples, 144 MPa. 10−30 μm brushite ($CaHPO_4$-$2H_2O$) Ca/P bioceramic coating of patented JDBM (Mg-Nd-Zn-Zr) alloy showed promising results with a bonding strength over 10 MPa [150]. Guan *et al.* [151] studied the *in vitro* and *in vivo* degradation of uncoated and brushite-coated Mg-based screws made of JDBM, *i.e.*, Mg-3.1wt.%Nd-0.2wt.%Zn-0.4wt.%Zr. The

screws were implanted in the mandible of New Zealand White rabbits. Figure 2 shows that degradation through as visualized by synchrotron radiation X-ray microtomography. Both the *in vitro* and *in vivo* results showed that the uncoated and brushite-coated screws are biocompatible. The *in vivo* degradation rates of the coated screws after 1, 4, and 7 months of implantation were 0.161 ± 0.075, 0.097 ± 0.013, and 0.218 ± 0.030 mm/year, respectively. Lichen *et al.* [152] prepared a composite coating by using micro-arc oxidation (MAO) on Mg substrates in an aqueous solution that included hydroxyapatite (HA) powder. Potentiodynamic polarization tests and immersion tests in SBF indicated that the specimens with the composite coating that were anodized in the HA-containing electrolyte have a better corrosion resistance than those anodized in the HA-free electrolyte. In another work, Dou *et al.* [153] prepared a porous bioceramic containing tricalcium phosphate (TCP) coating by MAO with different voltages on Mg-4.75wt.%Zn-0.55wt.%Ca alloy. The results indicate that the voltage have a noticeable influence on the thickness and corrosion properties of the bioactive TCP-containing MAO coating.
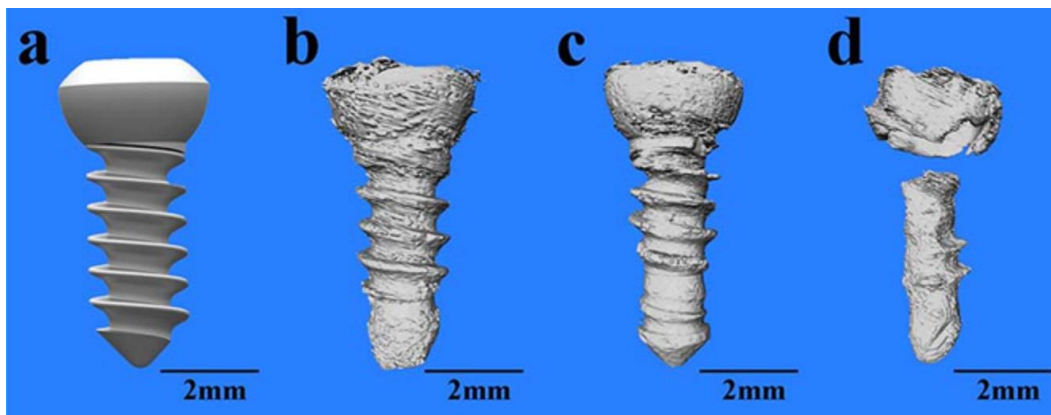

Fig. 2. Picture of original screw model (a) and 3D reconstruction images of C-JDBM screws after 1 (b), 4 (c), and 7 (d) months of implantation. No obvious degradation happened 1 month (b) post implantation. Slight volume loss was found 4 months (c) post implantation. Mg screw seriously degraded after 7 months (d) of implantation (adapted from [151]).

Biodegradable polymers such as poly lactic-co-glycolic acid (PLGA), Polylactic acid (PLLA), dichloromethane (DCM), and polycaprolactone (PCL) have also been used as a non-substrate-involving coating [25, 154-156]. It is well known that a PLGA coating improves corrosion resistance and enables cell adhesion and organization of the attached cell's cytoskeleton [154]. Li *et al.* [157] investigated the effect of sealing the surface pores of MAO-treated pure Mg samples with a layer of PCL creating a composite coating. The PCL layer was deposited by dipping the MAO-treated samples in 4 and 7 wt.% PCL solution for 1 min. The samples were then pulled out slowly at a rate of 20 mm/min. The results obtained from the immersion test and the potentiodynamic polarization test revealed that the porous nature of MAO-treated Mg alloys did not by itself reduce corrosion resistance in Hanks' balanced salt solution (HBSS). However, the deposition of PCL onto the MAO-treated surfaces significantly increased the corrosion resistance. Zomorodian *et al.* [158] developed a composite coating on the AZ31 alloy by adding nano hydroxyapatite particles and an antibiotic, cephalexin, to PCL. Although the addition of the nano hydroxyapatite particles and antibiotic resulted in reduced corrosion protection, the composite coating has enhanced biocompatibility and anti-bacterial functionality.

Sheng *et al.* [159] prepared hexamethylenediaminetetrakis (methylenephosphonic acid) (HDTMPA) surface-modified Mg alloy samples via a covalent immobilization process in conjunction with a sequential deposition process. HDTMPA is an organic phosphate that as a coating is biocompatible and provides corrosion resistance [159]. Electrochemical corrosion and immersion corrosion results reveal that the HDTMPA-coated Mg alloy

samples provides reduced corrosion. Razavi *et al.* [160] show that a nanostructured akermanite ($Ca_2MgSi_2O_7$) coating improves corrosion resistance and the surface bioactivity of the coated Mg alloys. These nanostructure coatings were grown on AZ91 Mg alloy samples through an electrophoretic deposition (EPD) process. Zhao *et al.* [161] used dual zirconium and oxygen ion implantation to create a rough, hydrophobic and ZrO_2-containing surface film on the magnesium–calcium (Mg–Ca) and magnesium–strontium (Mg–Sr) alloys. Through *in vitro* weight loss measurements and electrochemical corrosion testing of the coated alloy samples, it was shown that the coating increased corrosion resistance.

A compact fluoride conversion coating composed of MgO and MgF2 was applied to AZ31B alloy samples (Mg-3wt.%Al-1.1wt.%Zn-0.70wt.%Mn) by Yan et al [162]. Immersion and electrochemical test results showed an improved corrosion resistance for the coated alloy in SBF. Razavi *et al.* [163] combined micro arc oxidation (MAO) and electrophoretic deposition (EPD) to coat AZ91 alloy samples with CaMgSi2O6 nanostructured diopside. Electrochemical corrosion, immersion and compression test results showed that the diopside coating not only slowed down the corrosion rate, but also enhanced *in vitro* bioactivity, mechanical stability and cytocompatibility of the alloy. Zomorodian *et al.* [164] created a composite coating composed of a thin inner layer of polyetherimide (PEI), as an adhesion promoter between Mg substrate and a nanohydroxyapatite-modified PCL outer layer to provide corrosion protection on AZ31 alloy samples. Increasing the PCL concentration results in a better corrosion protection of the Mg alloy, while the presence of nanohydroxyapatite particles

enhances the cellular response over the coating and reduces the coating's corrosion resistance.

While a coating can control degradation timing, it should not undermine the stabilization function of the resulting implant. Tan *et al.* [73] used the extraction torque test to compare the interface strength between AZ31B screws and the surrounding host tissues of uncoated samples and samples with a Si-containing coating. The results were compared with those of surgical grade titanium (Ti6Al4V) and biodegradable PLLA bone fixation screws. After 4 weeks of implantation, the extraction torque was similar for all of the implanted screws (15-17 N.cm). The only exception was for the uncoated AZ31B screws with a torque of 5 N.cm. After 21 weeks of implantation, the extraction torque for the coated AZ31B was the highest (about 22 N.cm) while the PLLA screws had the lowest extraction torque (about 11 N.cm).

Sanchez *et al.* [165] is the only study we are aware of that attempts to correlate *in vitro* and *in vivo* results obtained from different Mg alloy coating studies. We recommend efforts be made to set standards for *in vitro* and *in vivo* coated alloy sample corrosion testing. Some of the discussed *in vitro* and *in vivo* work results in this section are listed in Table 3.

4. Manufacturing of Mg alloys

Mg alloys can be manufactured by various methods. The choice of a particular method depends on many factors such as the targeted component properties, shape, dimensions, the ability to cast an alloy and the number of parts to be synthesized [168, 169]. About 98% of structural applications of Mg are produced by casting [170]. Other processing techniques such as liquid infiltration, in situ processes, spray deposition and disintegrated melt deposition can be used to fabricate Mg matrix composites [171]. Mechanical treatment (*e.g.,* hot rolling, hot extrusion, equal channel angular pressing, deep rolling, low plasticity burnishing), machining (*e.g.,* polishing) and heat treatment (*e.g.,* age hardening) are post processing methods that may enhance the mechanical and corrosion characteristics of Mg alloys [15, 32, 35, 172-175]. Oxidation can be minimized during fabrication by using an inert gas (*e.g.,* argon) especially for high temperature procedures [13, 37, 38]. An Mg alloy powder can ignite at lower temperatures and, therefore, handling safety should carefully be planned. This section deals with fabrication techniques to achieve alloys with desired mechanical properties and corrosion performance.

4.1. Mg Alloy Casting

Casting is the predominant method for Mg alloys parts production [176]. High productivity, high precision, and high surface quality are some of the reasons these parts are prepared by casting [169]. From materials science point of view, casting is the first fabrication process that assures the formation of secondary phases due to complete melting and efficient mixing of all alloying elements. Typical Mg-based medical devices would be firstly cast with a designed chemical composition, and they can then undergo different kinds of post-casting processes and treatments to obtain the desired part shape and/or to improve their properties (e.g. mechanical treatment, heat treatment and machining) [15, 27, 41, 177, 178]. High pressure die casting (HPDC), as well as, gravity casting has been used in addition to more recent methods of low pressure casting, squeeze casting, semi-solid casting, lost foam casting and ablation casting [179-181]. We will discuss the most common casting methods in this section.

Table 3 The *in-vitro* and *in-vivo* corrosion characteristics and biocompatibility for different coatings created on Mg alloys.

Coating type	Alloy type	Coating process	*In vitro* electrochemical corrosion test (SBF)			*In vitro* cytotoxicity	*In vivo* corrosion test		Ref.
			Corrosion potential E_{corr} (μv vs. SCE)	Current density i_{corr} (μA/cm²)	Calculated corrosion rate (mm/year)		Tissue response	Calculated corrosion rate (mm/year)	
Magnesium oxide[a]	Mg-Ca	Alkaline oxidation by soaking in NaHCO$_3$ for 24 h, then annealing at 773 K for 12 h	-1930 (coated) -1560 (uncoated)	39.8 (coated) 316 (uncoated)	2.29 (coated) 13.27 (uncoated)	No toxicity to L-929 cells	-	-	[135]
Magnesium oxide	AZ31B	MAO in 30 g/L Na3PO4 at 325 V for 5 min at 3000 Hz and 0.3 pulse ratio	-1150 (coated) -1300 (uncoated)	3.09 (coated) 101 (uncoated)	0.036 (coated) 2.3 (uncoated)	-	-	-	[166]
Ca-def HA	Mg-Zn-Ca	Pulse electrodeposition at 85 °C, 20 mA/cm² current density, 0.5 duty cycle for 30 min	-	-	-	-	Remarkable proliferation of osteoblast and new bone formation after implantation into rabbit femora	0.15 (coated) 0.8 (uncoated)	[167]
Brushite[b] (CaHPO$_4$·2H$_2$O)	Mg−Nd−Zn−Zr (extruded)	Immersion in 0.1 M KF for 24 h, then in NaNO$_3$ + Ca(H$_2$PO$_4$)$_2$·H$_2$O + H$_2$O$_2$ for 24 h	-1590 (coated) -1600 (uncoated)	1.17 (coated) 1.57 (uncoated)	0.253 (coated) 0.337 (uncoated)	No toxicity toMC3T3-E1 cells and bone marrow mesenchymal stem cells responded positively	Newly formed bone was observed around screws and a protective layer of bone-like apatite formed after implantation into mandible bones of rabbits	0.161 (coated)	[150], [151]
PLGA[c]	Mg-Zn (extruded)	Immersion in 4% PLGA powder in chloroform solvent until solvent evaporated	-1360 (coated) -1460 (uncoated)	0.097 (coated) 26.7 (uncoated)		the mouse osteoblast-like MC3T3 cells could develop enhanced confluence on and interactions with the coated samples	-	-	[154]
HDTMPA	Pure Mg	Immersion in 10 mM of HDTMPA solution (pH 6) at 60 °C for 40 min	-1620 (coated) -1580 (uncoated)	5.43 (coated) 4.36 (uncoated)		CaP precipitation as well as osteogenic prompted osteoblast cells proliferation	-	-	[159]
Nan-diopside (CaMgSi$_2$O$_6$)	AZ91	MAO in NaOH + Na2SiO3 solution at 60 V and 30 min, then EPD in (CaMgSi$_2$O$_6$) suspension at 100 V and 3 min	-1480 (coated) -1600 (uncoated)	0.11 (coated) 6.31 (uncoated)		Relatively stable interface for cell viability/adhesion and slow release of corrosion products after coating.	-	-	[163]
Si-containing coating[d]	AZ31B (extruded)	Acidic etching, then immersion in NaOH + Na$_2$SiO$_3$ + Na$_4$P$_2$O$_7$ for 120 h at 60 °C	-1160 (coated) -1230 (uncoated)	0.51 (coated) 11.34 (uncoated)	0.011 (coated) 0.248 (uncoated)	Showed no systemic toxicity and sensitization. Rank: 0 in cytotoxicity, hemolytics and rank: <1 in irritation	bone–implant interface strength of coated AZ31B increased with implantation time into rabbit femora	-	[73]

[a] The corrosion potential and current density were deduced from Fig. 8 in Ref. [135].

[b] The *in vitro* corrosion and cytotoxicity test results were obtained from Ref. [150], the corrosion test was conducted in Hank's solution.

[c] The *in vitro* corrosion test was conducted in 0.9% NaCl solution.

[d] The *in vitro* corrosion test was conducted in Hank's solution.

High pressure die casting (HPDC) is the dominant method of casting Mg alloy parts [182]. There are two types of HPDC: hot chamber die casting and cold chamber die casting [170]. High productivity and precision, excellent surface quality, and the possibility of fabricating thin walls and complex structures are the main advantages of HPDC [182, 183]. The main drawbacks of this method are the limited range of alloys available, the difficulty of heat treatment and the formation of pores from trapped gas due to the high fill-up-rate and solidification process [169, 184]. To minimize the effect trapped gas and produce less porous parts, vacuum-assisted die casting [170, 185, 186] and super vacuum die casting [187, 188] have been used. These processes are more costly and offer lower production rates [170, 185]. In the hot chamber die casting method, molten metal is kept in an enclosed steel crucible under a protective atmosphere to minimize the formation of harmful oxides as shown in Figure 3.a. [185]. The cold chamber die casting process is shown in Figure 3.b. [185]. In this procedure, molten Mg is conducted into a shot cylinder by a pump, auto-ladling or by hand ladling. It is then injected into the cavity to solidify under pressure. Cold chamber casting has several distinct advantages such as cost effectiveness which minimizes the chance of a reaction between Mg and the die material, and air; fabricating large parts due to the fast injection of metal into the cavity; and, the production of very fine grains due to a rapid solidification process [170, 185, 189].

Gravity casting is usually performed in sand or a permanent metallic molds [183]. Mg parts of up to 1400 kg have been cast by the sand casting process (*e.g.,* green sand, CO_2/silicate or resin-bonded sand) [176, 190]. Permanent Mold Casting (PMC) has

several advantages over sand casting such as fine surface, precise and consistent dimensional control and improved mechanical properties. However, there are also some limitations on the variation of the shapes that can be produced by permanent mold casting [170, 191, 192].

Low pressure casting (LPC) is illustrated in Figure 3.c. A typical LPC machine comprises a pressurized crucible with a feed tube (riser tube) running from the crucible to the bottom of the mold [179]. The most significant advantage of this method over HPDC is that it can create hollow structures that cannot be produced by HPDC [179]. However, the low pressure casting has some drawbacks. For example, it cannot produce Mg structures with wall thicknesses below 3 mm [193].

1.1. Mechanical treatments

Mechanical treatments (*e.g.,* cold working and hot working processes) are secondary processing techniques that have been used to improve Mg alloy mechanical properties and corrosion characteristics. The mechanisms for these improvements include stacking faults, refining the grain size and introducing higher density dislocations [27]. There are several ways to mechanically treat Mg alloys such as extrusion, rolling (sheet forming), deep drawing and forging. Hot rolling and hot extrusion are the most common techniques. Hot rolling has been found to reduce the corrosion rate of Mg-Ca alloys by decreasing grain size (refining) [41]. In general, hot extrusion requires a larger extrusion ratio, smaller load, and higher speed than cold extrusion. The extrusion speed, temperature and load may significantly affect the properties of hot-extruded Mg alloys [194].
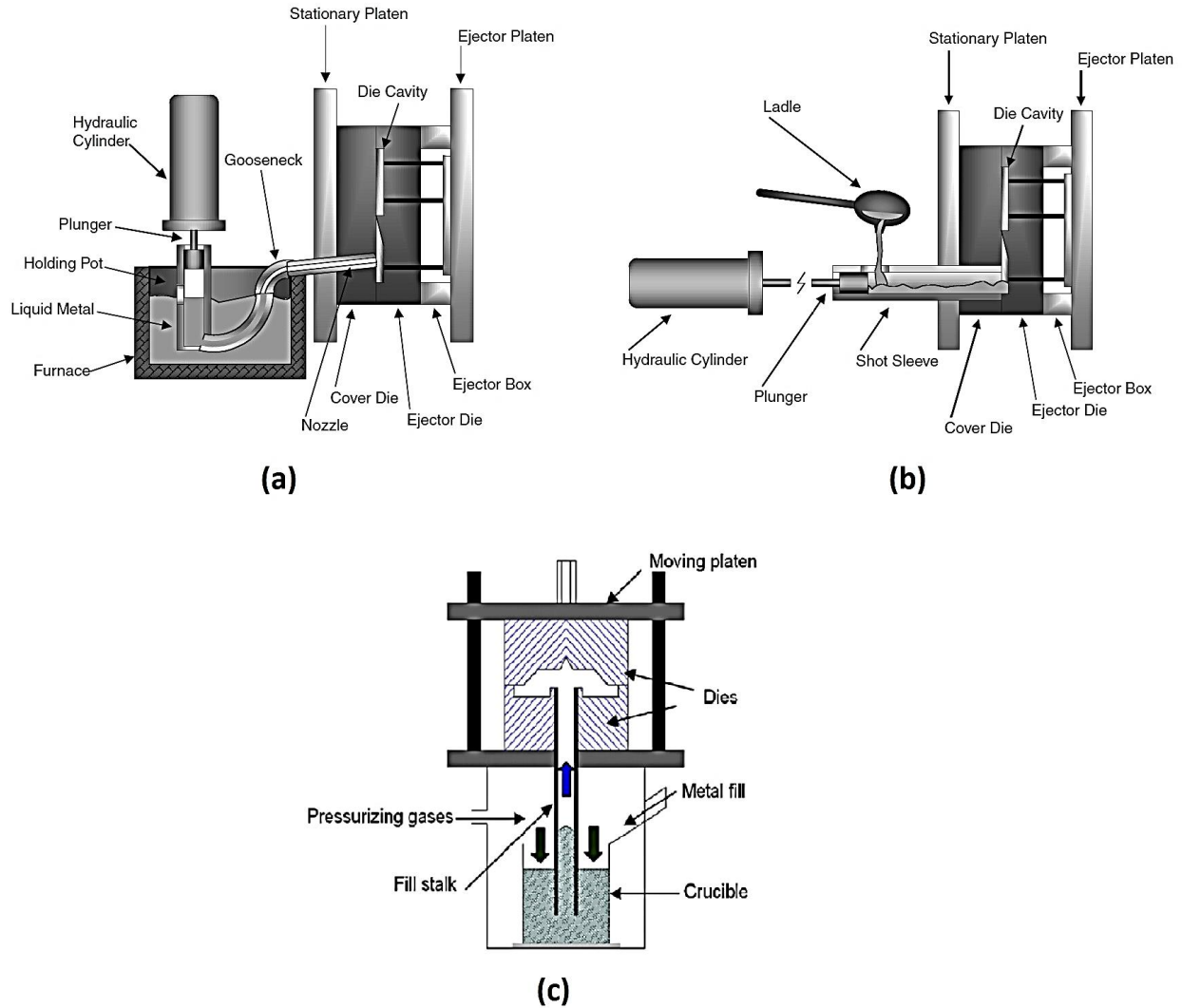
Fig. 3. Schematic diagrams illustrating different types of casting methods; (a) hot chamber die casting (adapted from [185]); (b) cold chamber die casting (adapted from [185]); (c) low pressure casting (adapted from [179]).

Li *et al.* [195] studied the effects of different extrusion conditions on the mechanical and corrosion properties of a Mg–2wt.%Nd–0.2wt.%Zn alloy (NZ20). The alloys that were preheated and extruded at lower temperature had relatively lower corrosion rate and higher yield strength in comparison to those extruded at a higher temperature. In another study, Li *et al*. [35] investigated the effect of hot rolling and hot extrusion on the mechanical and corrosion performance of Mg-Ca alloys. The tensile strength

was increased from 71.38 MPa for the as-cast Mg-1wt.%Ca alloy to 166.7 MPa and 239.63 MPa for the hot-rolled and hot-extruded alloys respectively. Cha *et al.* [41] investigated the effect of hot extrusion on refining the grain size of pure Mg; they found that the grain size can be reduced to 25 µm for pure Mg and to 10 µm for the Mg-5wt.%Ca-1wt.%Zn alloy (grain size of as-cast pure Mg is around 875 µm) [175]. Cha *et al.* [41] added 1 to 5wt.%Zn to the as-cast and the extruded Mg-5wt.%Ca alloy. In their *in vivo* tests on

Sprague–Dawley rats, H_2 bubbles were formed during the first week after surgery and persisted for 12 weeks in the case of the as-cast plates. On contrary, no H_2 bubbles were observed for the implanted extruded plates. These results were similar to *in vitro* Hydrogen evolution tests. In a related *in vivo* study of New Zealand-white rabbits for 24 weeks, new bone formation was observed for an extruded Mg-5wt.%Ca-1wt.%Zn alloy implanted sample with no observation of H_2 bubbles [41].

Deep Rolling (DR) and Low Plasticity Burnishing (LPB) are two of the cold working processes that have been performed on Mg alloys. The cold working leads to compressive residual stresses that improve the corrosion resistance by means of cracking and pitting prevention [1]. Denkena *et al.* [196] showed that high subsurface residual stresses induced by large plastic deformations during deep rolling reduce the corrosion rate by a factor of approximately 100 times for a Mg-3wt.%Ca alloy. However, excessive values of residual compressive stresses are not recommended in order to avoid workpiece surface deterioration and microstructural upper layer damage [196]. The effect of grain refinement on the AZ31 alloy corrosion behavior as a results of different fabrication techniques was investigated by Wang *et al.* [172]. Squeeze casting (SC), hot rolling (HR), and equal channel angular pressing (ECAP) processes were performed on AZ31 resulting in grain sizes of 450 µm, 15 µm and 2.5 µm, respectively. The degradation rates in Hank's solution of the HR and ECAP prepared samples were significantly lower than that for the SC prepared samples, as shown in Figure 4. For example, the degradation rate of the SC prepared samples was approximately 1.56 µm/day while it was about 1.25 µm/day for both the HR and ECAP prepared samples. Ratna Sunil *et al.* [197]

studied the *in vitro* and *in vivo* degradation behavior of AZ31 alloy processed by ECAP at 300 °C for up to four passes. The grain size was reduced from 46 µm to 1-5 µm after the ECAP process and the alloy samples processed for 4 passes showed the lowest corrosion rates of approximately 6mm/year after 27 h of *in vitro* immersion and 1.1 mm/year after 60 days of *in vivo* implantation. Zhang *et al.* [198] investigated the *in vitro* corrosion behavior of biomedical Mg–Zn–Ca alloy produced by high pressure torsion (HPT) up to 5 revolutions at room temperature and 7.5 GPa. It was observed that the HPT process caused grain refinement from 11 µm to 130-150 nm and a uniform distribution of the secondary phase. These microstructural variations resulted in a uniform corrosion rate and mode.
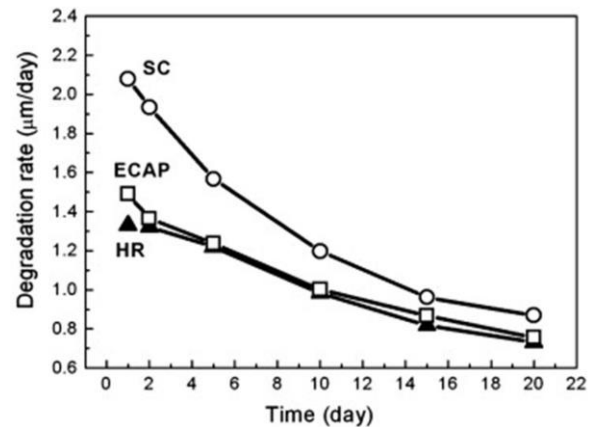

Fig. 4. Degradation rate in Hank's solution of the three material states investigated (adapted from [172]).

1.2. Heat treatment

Heat treatment involves heating and cooling of Mg alloy part in its solid state, normally to extreme temperatures and at various heating/cooling times and rates, to obtain enhanced mechanical and corrosion properties. Heat treatment of Mg alloys includes different processes such as solution

treatment, annealing, quenching and age hardening (precipitation hardening) [15, 177]. If final Mg alloy parts have complex shapes such as porous structures, it may not be possible to perform mechanical treatment. In these cases, heat treatment may be used to strengthen final parts by means of intermetallic precipitation. The production of alloy microstructures containing uniform fine dispersions of thermally stable intermetallic precipitates is a practical approach for enhancing Mg alloys' strength, creep and corrosion resistance [177]. For example, such microstructures can be obtained for Mg-Ca-Al based alloys by mechanisms of precipitating stable eutectic phases such as Al_2Ca [177, 199].

The degradation behavior of heat-treated and untreated die-cast AZ63 alloy (Mg–5.9wt.%Al–3.5wt.%Zn–0.18wt.%Mn) after 14 days immersion in SBF was studied by Liu $et\ al.$ [32]. They found that the corrosion rate of the solution treated (at 413 °C for 24 h) then age hardened (at 216 °C for 5.5 h) AZ63 alloy is approximately half of the untreated alloy. In another study, the heat-treated Mg-2Mn-xCa (x=0.8, 1.0, 1.2 wt.%) alloys that were solution-treated and age-hardened showed superior mechanical and corrosion properties than the as-cast alloys [200]. This can be attributed to the transformation of the Mg_2Ca and α-Mn phases into dispersed fine precipitated phases. However, for some other Mg alloys, heat treatment may result in lower corrosion resistance in chloride solutions [12, 201].

Age hardening (precipitation hardening) of Mg-Ca alloys can be enhanced by the addition of elements such as Al and Zn [177, 199]. New Mg-Zn-Ca alloy enhanced mechanical properties after age hardening are due to the refinement and uniform distribution of

the α-Mg+$Ca_2Mg_6Zn_3$ eutectic phase into fine dispersions. However, excess presence of $Ca_2Mg_6Zn_3$ phase in Mg-Zn-Ca alloys, due to the high loading of Zn, suppresses the formation of finely dispersed monolayer Guinier-Preston (G.P.) zones on basal planes (0001) of the Mg hexagonal-closed-packed (HCP) unit cell. This leads to less age hardening effect [15, 120]. G.P. zones in Mg-Zn-Ca alloys are extremely fine (less than 10 nm) Zn and/or Ca enriched solute regions that form during age hardening [15]. The presence of G.P. zones result in physical obstructions to the motion of dislocations leading to improved mechanical properties [202]. The atomic ratio of Ca:Zn resulting in the formation of these ordered G.P. zones are between 1:1 and 1:2 [15]. Nie and Muddle [177] heat treated Mg-1wt.%Ca-1wt.%Zn (Zn/Ca = 0.61) alloy by water quenching from 470 ºC, then aging in an oil bath at 200 ºC for different aging durations. The maximum hardness achieved for the alloy was measured as 63 Vickers hardness (HV) for an aging time of 2 hours.

Mg-1wt.%Ca-1wt.%Zn was alloyed by casting, annealed for 5 hours at 315 ºC and solution treated for 24 hours at 480 ºC [203]. The alloy was then quenched in water (70 ºC), and finally age hardened in an oil bath at 200 ºC for different durations. The alloy aged in oil for 2 hours had the peak hardness, yield strength (YS) and ultimate tensile strength (UTS) of 63 HV, 131 MPa and 173 MPa respectively, with enhanced creep properties [203]. Bettles $et\ al.$ [204] studied the effect of age hardening on the mechanical properties ($i.e.$, tensile strength and creep) of Mg-0.1wt.%Ca-4wt.%Zn (Zn/Ca = 24.5). The alloy was solution treated at 618 K for 8 hours, then ramped over 2 hours to 732 K, with an immediate cold water quenching, then aged in oil bath at 450 K. The YS of this age-hardened alloy was

135 MPa with UTS of 263 MPa and 11% elongation. The precipitation hardening of Mg-0.3Ca-0.3Zn in atomic % (at.%) alloy of as-cast alloy samples was done by solution treatment at 773 K for 2 hours in He-filled Pyrex tubing, then water quenched, and finally dipped in oil bath at 473 K for different durations [205]. The formation of a pair of basal precipitates with a length of 5-7 nm brought about enhanced alloy hardness at longer aging durations. The effect of the Zn% in the age hardening response of Mg-0.3%Ca-x%Zn (in at.%) alloy after aging in an oil bath at 200 ℃ for different durations resulted in a peak hardness of 69 HV at 0.6% Zn content (Mg-0.5wt.%Ca-1.6wt.%Zn) and 2 hours aging duration [15]. Lu *et al.* [206] studied the effect of changing the

grain size and $CaMg_6Zn_3$ phase volume fraction of Mg-3wt.%Zn-0.3wt.%Ca alloy, due to solution treatment and quenching, on its *in vitro* corrosion resistance. They found that corrosion resistance after the heat treatment process and the minimum corrosion rate was observed in the alloy solution treated at 420 °C for 24 h. Table 4 shows the processing history and the resulting properties of Mg-Ca, Mg-Zn and Mg-Zn-Ca alloys. The main parameters that controls the formation of the Mg-Zn-Ca alloy microstructure phases are the Zn%, Ca% and Zn/Ca atomic ratio. Hence, the corrosion performance and precipitation hardening are also significantly affected by these parameters.

Table 4. The processing history, mechanical properties and corrosion rate of Mg-Ca, Mg-Zn and Mg-Zn-Ca alloys.

Alloy composition (%wt.)	Processing history	0.2% Yield strength (MPa)	Tensile strength (MPa)	Elong. (%)	*In vitro* electrochemical corrosion rate (mm/year)	Ref.
Mg-1%Ca	As-cast	40	71	1.8	12.56 (SBF)	[35]
Mg-1%Ca	Hot rolled (400 °C, from 5 to 2 mm)	120	166	3	1.63 (SBF)	[35]
Mg-1%Ca	Hot extruded (210 °C, 17:1)	135	239.5	10.6	1.74 (SBF)	[35]
Mg-6%Zn	solution treated (350 °C, 2 h) + quenched + Hot extruded (250 °C, 8:1)	169.5	279.5	18.8	0.16 (SBF)	[37]
Mg-4%Zn-0.2%Ca	solution treated (400 °C, 5 h) + quenched + Hot extruded (270 °C, 16:1)	240	297	21.3	1.98 (SBF)	[42]
Mg-4%Zn-0.1%Ca	solution treated (618 K, 8 h) + quenched + age hardened (oil, 450 K, ~2 days)	135	263	11	-	[204]
Mg-1%Zn-1%Ca	Annealed (315 °C, 5 h) + solution treated (480 °C, 24 h) + quenched + age hardened (oil, 200 °C, 2 h)	131	173	3	-	[203]

When Mg-Zn-Ca alloy is heat treated for use as bone fixation, three important factors about chemical composition should be considered: (i) the Ca content should not exceed its solubility limit (1 wt.%) in Mg to avoid excess formation of Mg_2Ca and since further increase in Ca content does not cause more grain refinement (*e.g.,* 0.5wt.%Ca in the Mg-Zn-Ca-Mn alloying system) [12, 35, 41], (ii) the Zn content should be below 5 wt.% since at higher Zn loading, corrosion resistance deteriorates [41, 60], (iii) the Zn/Ca atomic ratio should be in the range of 1.2 to 2.0 since this is the range for optimum corrosion resistance, and age hardening effect [15, 35, 120].

1.3. Machining

Different types of machining processes can be used with Mg alloys to reach the desired final shape, size and surface quality such as turning, milling, grinding and polishing. The surface finish quality after machining processes has a significant effect on the corrosion performance of Mg alloys [196]. Höh *et al.* [207] found that smooth surface finish reduces pitting corrosion and provides the best integration in bone compared to a rough surface finish. Yue *et al.* [178] studied the effect of surface finish after four different machining processes on the corrosion behavior of Mg ZM51/SiC composite. The employed machining processes were single-point diamond turning (SPDT), wire electrical discharge machining (WEDM), grinding and polishing. As seen in Figure 5, the surface finish quality had a significant effect on the Mg ZM51/SiC composite's *in vitro* corrosion characteristics. The highest corrosion resistance was observed after polishing and fine grinding. It should be mentioned that the use of cutting fluids during machining Mg components is known to reduce surface roughness although Mg alloys are traditionally machined dry [208].
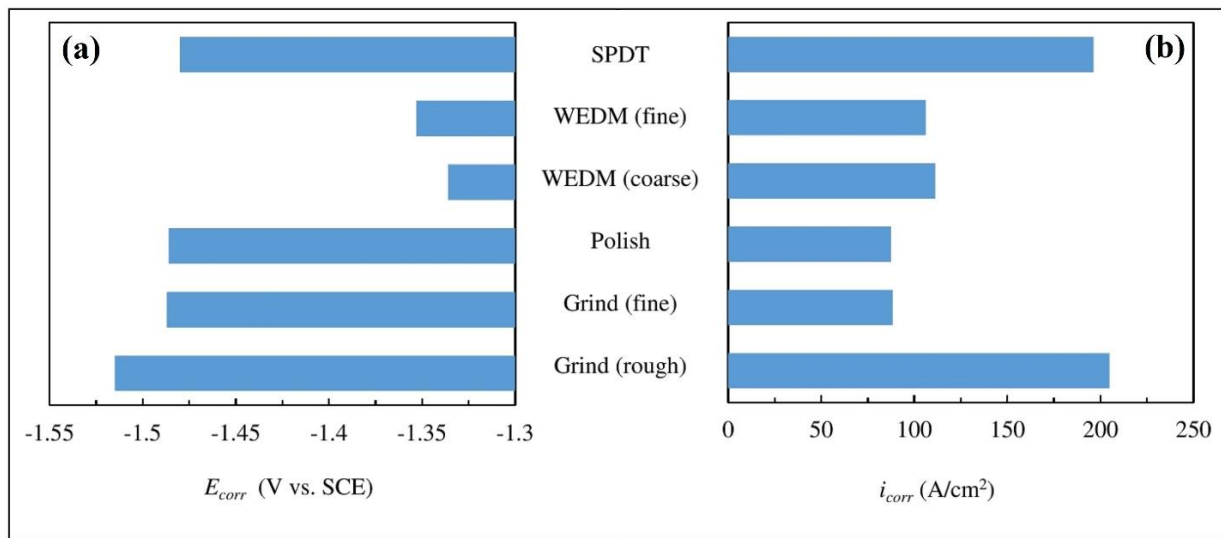

Fig. 5. The calculated Potentiodynamic polarization test corrosion properties for various machined specimens of Mg ZM51/SiC composite: (a) corrosion potential (E_{corr}), (b) corrosion current density (i_{corr}). Fine grinding and polishing showed the highest corrosion resistance (values were deduced from [178]).

1.4. Additive manufacturing

Patient-specific biodegradable-metallic fixation hardware could reduce operating time and result in better treatment outcomes. It is expected that 3D printing (*i.e.*, additive manufacturing or AM) of resorbable fixation devices will be a significant clinical breakthrough. AM has only recently be shown useful to create fixation hardware with controlled geometry density, surface morphology, mechanical properties, and corrosion rates [17]. One of the first efforts towards additively manufacturing Mg used selective laser melting (SLM) [209]. In SLM process, fine Mg or Mg alloy powder is diffused together, layer by layer, using high power laser beam to create a 3D Mg-based part [210]. A GSI Lumonics Marker SPe Nd:YAG laser was used with a scanning speed of 0.2-300 mm/s. Two types of pure Mg powder were processed: spherical grains (75-150 µm) and irregular-shaped grains (5-45 µm). Unlike coarse powders, fine powders were found to melt and sinter without agglomeration for energy densities up to 0.66 J/mm^2 [211]. It was shown that the surface morphology and dimension characteristics of pure Mg specimens were affected by the laser's wave mode (pulsed or continuous). Under pulsed mode, pulse duration was fixed at 20 ns and the repetition rate (frequency) varied between 10 and 60 kHz. Increasing the pulse frequency resulted in further reduction in laser's peak energy from 130 kW to 22 kW at 10 kHz and 60 kHz, respectively. Also, energy density has a significant effect on the presence of porosity and cracks thus, the quality of a SLM Mg part. Relatively smooth, flat surfaces can be produced by 3D printing. Depending on the energy density, porosity and cracks are observed. Unlike a pulsed laser, specimens fabricated by continuous

wave irradiation showed a disrupted surface and smooth, regular beads [211]. In another study the mechanical properties and microstructural characteristics of SLM-printed Mg were investigated [212]. They found grain size increased as the energy density increased, as seen in Figure 6. This caused the hardness and modulus of the printed Mg to decrease from 0.95 to 0.59 GPa and from 33 to 27 GPa, respectively. Savalani *et al.* [213] probed the influence of preheat and the thickness of layer in selective laser melting of Mg. The results showed that preheating improves the quality of the surface in conjunction with creating a better bonding to the surface. Also, low layer thicknesses resulted in smoother and flatter surfaces (low surface roughness). Matena *et al.* [214], used SLM to produce porous Mg implants coated with PCL to decrease their corrosion rate. The results showed reduction in the corrosion rate and good biocompatibility of the SLM produced magnesium coated with PCL.

As expected, the success of SLM in fabricating Mg-based implants requires overcoming the challenges related to powder handling. Mg alloys have a very high oxygen affinity. This is exacerbated in its powder form due to the increased surface area per volume. Molten Mg has a low dynamic viscosity (1.5 Pa·s) compared to molten titanium (2.2 Pa·s). The small difference between Mg's melting point (650 ℃ for pure Mg) and vaporization point (1090 ℃ for pure Mg) at atmospheric pressure, (ca 440 ℃ for pure Mg), also present significant challenges for powder production and handling [215]. The low dynamic viscosity of Mg may cause spatter and porosity, and a further decrease in the viscosity will undermine laser-melted Mg track formation [216].
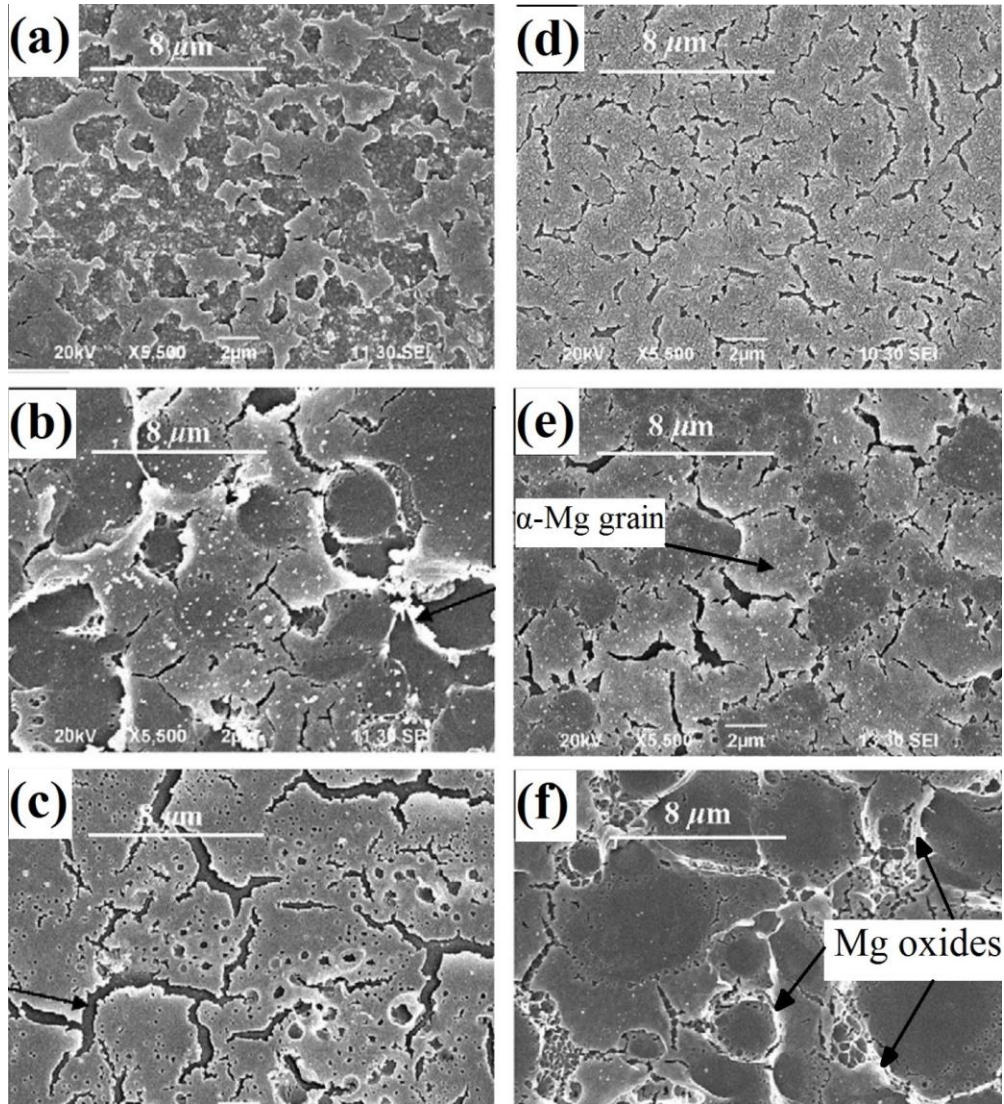
Fig. 6. Scanning electron microscopy (SEM) of Mg powder surface morphology which was processed under pulse wave irradiation at three energy density values (a) 1.13×10^{12} J/m^2; (b) 3.27×10^{12} J/m^2; (c) 9.80×10^{12} J/m^2 and under continuous wave irradiation at three energy density values (d) 1.27×10^9 J/m^2; (e) 3.92×10^9 J/m^2; (f) 7.84×10^9 J/m^2 [212].

It is therefore, important to choose proper process parameters, so the level of the input energy and the melt temperature are not high. Hence, an excessive, problematic, decrease in dynamic viscosity can be avoided. The small difference between the melting and vaporization points results in an increased powder "balling" tendency. An additional adverse effect is in the deposition of Mg vapor on the surfaces of the SLM chamber [217-219]. A possible solution to this problem would be increasing the pressure of the processing chamber. At pressure of 3 bars, the temperature difference between the melting point (ca 650 ℃) and the vaporization points (1220 ℃) for pure Mg can increase from 440 ℃, at

atmospheric pressure, to 570 ℃ as depicted in Figure 7 [217, 220]. Using this approach, the research team at the Fraunhofer Institute for Laser Technology (ILT) has succeeded in additively manufacturing the commercial AZ91 alloy using SLM. The resulting parts have a density greater than 99 percent. During the process, the oxygen content of the inert gas atmosphere was successfully controlled below 10 ppm to eliminate the chance of oxidation due to the high oxygen affinity of Mg and Mg alloys [221]. Roland *et al.* [222] succeeded to create porous Mg samples using SLM with highest possible resolution achieved of 600 µm. Similar Mg porous structures were fabricated by Matena *et al.* [214] by SLM. The samples were then coated with PCL and their biocompatibility was compared with titanium scaffolds fabricated by SLM and coated with PCL. The live cell imaging showed similar seeding densities for Mg and titanium samples until the second day. After two days, Mg samples showed decreased cell number. Also, the *in vitro* corrosion testing for the PCL-coated Mg samples showed enhanced corrosion resistance compared to non-coated Mg samples [214]. It is also possible to 3D print porous Fe-Mn scaffolds using a powder based binder jet printing [223]. These Fe-Mn alloy scaffolds demonstrated good cytocompatibility compared to tissue culture plastic with tensile mechanical properties similar to natural bone and corroded much faster than those made of pure iron [224].
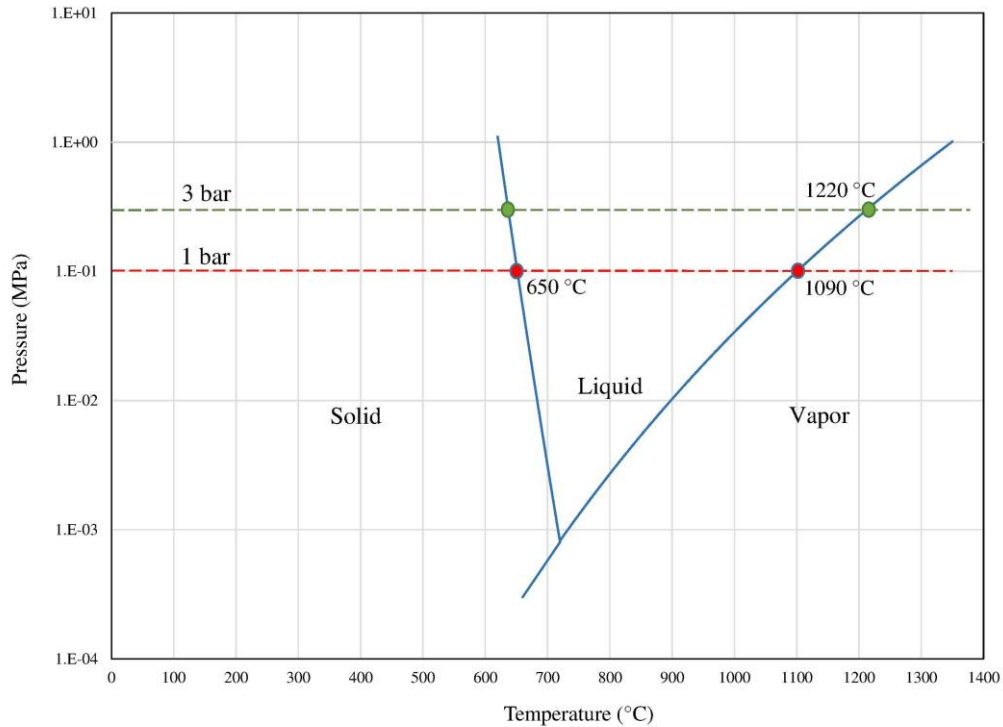

Fig. 7. Schematic unary phase diagram for pure magnesium, showing the melting and vaporization points at two pressure levels (1 bar and 3 bar), increasing the pressure from one atmosphere pressure (1 bar) to 3 atmosphere pressure (3 bar) increases the difference between the melting and vaporization temperatures from 440 ℃ to 570 ℃ which results in less powder balling tendency [215, 217, 220].

28

2. Conclusions

Ultimately, the aim of this work is to guide future investigators toward developing successful resorbable bone fixation hardware by covering the topics of resorbable bone fixation characteristics and the progress in property improvements by alloying, coating, and possible fabrication techniques. Biodegradable alloys hold promise for bone fixation hardware. However, these biocompatible alloys, especially Mg alloys, with acceptable mechanical and corrosion properties, as well as viable fixation device fabrication methods, are beginning to be tested in experimental settings. Resorbable fixation that can carry the body's load and then safely resorb would be a significant clinical breakthrough. Several Mg alloys are resorbable and offer promising alternatives to resorbable polymers due to their relatively greater strength, higher implant stability, and better osseointegration.

The process of developing patient-specific biodegradable Mg fixation hardware can start from an FEA of the bone to be repaired and design of optimal fixation mechanical properties and geometry in early stages. Mg, Ca, Zn and Mn alloys are among the most resorbable and biocompatible metals available for these applications. Coatings can prevent resorption of an Mg alloy fixation device until the initial phase of bone healing is completed. The selection and designing of the appropriate coating that will resorb at a highly predictable rate, prevent biofilm formation, and possibly deliver antibiotics has yet to be identified. Other factors that should be considered are implantation location and the interaction between the coating and the Mg alloy substrate. Carefully designed comparative coating studies would be helpful. To this end, there is a need for standards for the *in vivo* and *in vitro* Mg alloy fixation device corrosion and mechanical tests. Another area that requires attention is the corrosion behavior of coated and heat-treated Mg alloys. Equally important is a more comprehensive investigation of 3D-printing as a fabrication technique for patient-specific Mg alloy fixation devices.

Casting is the prevalent fabrication method for Mg alloys; HPDC is the most dominant casting method due to its high production rate and excellent surface quality. Mechanical treatments such as hot rolling, hot extrusion, and deep rolling can be used to enhance the mechanical and corrosion characteristics of the resulting parts. Heat treatment (*e.g.,* age hardening) is an effective way to improve the Mg alloys mechanical properties as in the case of Mg-Zn-Ca alloys. In addition to Zn and Ca contents, the Zn/Ca ratio significantly affect the number of intermetallic compounds that precipitate and, therefore is the most influential parameter controlling the resulting fixation device mechanical properties, corrosion performance, and age hardening affects. Surface finish quality has a significant effect on the corrosion and bone-implant contact of Mg alloy fixation devices.

Funding

Acknowledgment

References

1. Salahshoor, M. and Y. Guo, *Biodegradable orthopedic magnesium-calcium (MgCa) alloys, processing, and corrosion performance.* Materials, 2012. **5**(1): p. 135-155.
2. Bone, U.S. and J. Decade, *The burden of musculoskeletal diseases in the United States.* Rosemont, IL: American Academy of Orthopaedic Surgeons, 2008.
3. Stuart I. Weinstein, E.H.Y. *Prevalence of Select Medical Conditions - United States Population.* 2013 [cited 2016 4 April]; Available from: http://www.boneandjointburden.org/2014-report/ib0/prevalence-select-medical-conditions.
4. *United States Bone and Joint Initiative: The Burden of Musculoskeletal Diseases in the United States (BMUS), Third Edition, 2014. Rosemont, IL. [cited 2016 05 May]; Available from http://www.boneandjointburden.org.*
5. The American Academy of Orthopaedic Surgeons. *Internal Fixation for Fractures.* 2014 [cited 2014 19 Jan]; Available from: http://orthoinfo.aaos.org/topic.cfm?topic=A00196.
6. Transparency Market Research, *Orthopedic Trauma Fixation Devices Market Analysis, Market Size, Application Analysis, Regional Outlook, Competitive Strategies And Forecasts, 2014 To 2020*. 2014. p. 94.
7. University of Cambridge. *Structure of bone and implant materials.* 2011 [cited 2015 4 Jan]; Available from: http://www.doitpoms.ac.uk/tlplib/bones/index.php.
8. Huang, Z.-M. and K. Fujihara, *Stiffness and strength design of composite bone plates.* Composites science and technology, 2005. **65**(1): p. 73-85.
9. Rahmanian, R., et al., *Load bearing and stiffness tailored NiTi implants produced by additive manufacturing: a simulation study*, in *The International Society for Optical Engineering.* 2014: San Diego, California.
10. Slowik, G. *Do metal plates and screws need to be removed from the bone after a fracture has healed.* 2013; Available from: http://ehealthmd.com/blog/should-metal-plates-and-screws-or-nail-hardware-be-removed-bone-now-my-fracture-has-healed#axzz4A6XaUzHM.
11. Manivasagam, G. and S. Suwas, *Biodegradable Mg and Mg based alloys for biomedical implants.* Materials Science and Technology, 2014. **30**(5): p. 515-520.
12. Kirkland, N.T. and N. Birbilis, *Magnesium Biomaterials: Design, Testing, and Best Practice.* 2014: Springer.
13. Chen, Y., et al., *Recent advances on the development of magnesium alloys for biodegradable implants.* Acta biomaterialia, 2014. **10**(11): p. 4561-4573.
14. Tan, L., et al., *Biodegradable materials for bone repairs: a review.* Journal of Materials Science & Technology, 2013. **29**(6): p. 503-513.
15. Oh-Ishi, K., et al., *Age-hardening response of Mg–0.3 at.% Ca alloys with different Zn contents.* Materials Science and Engineering: A, 2009. **526**(1): p. 177-184.
16. Staiger, M.P., et al., *Magnesium and its alloys as orthopedic biomaterials: a review.* Biomaterials, 2006. **27**(9): p. 1728-1734.
17. Andani, M.T., et al., *Metals for bone implants. Part 1. Powder metallurgy and implant rendering.* Acta biomaterialia, 2014. **10**(10): p. 4058-4070.
18. Elahinia, M., et al. *Site-specific Material Properties And The Additive Manufacturing Of Nitinol Musculoskeletal Implants.* in *TISSUE ENGINEERING PART A*. 2014. MARY ANN LIEBERT, INC 140 HUGUENOT STREET, 3RD FL, NEW ROCHELLE, NY 10801 USA.
19. Moghaddam, N.S., M. Elahinia, and D. Dean, *A New Method to Support Both the Immobilization Needed During Healing and the Distribution of Strain through the Engrafted Bone Once it has healed*, in *Midwest American Society Biomechanics Regional Meeting*. 2015: Akron, Ohio.
20. Witte, F., *The history of biodegradable magnesium implants: a review.* Acta Biomaterialia, 2010. **6**(5): p. 1680-1692.
21. Lambotte, A., *L'utilisation du magnesium comme materiel perdu dans l'osteosynthè se.* Bulletins et Me´mories de la Socie´ te´ National de Chirurgie, 1932. **28**: p. 1325–1334.
22. Zheng, Y., X. Gu, and F. Witte, *Biodegradable metals.* Materials Science and Engineering: R: Reports, 2014. **77**: p. 1-34.
23. Noviana, D., et al., *The effect of hydrogen gas evolution of magnesium implant on the postimplantation mortality of rats.* Journal of Orthopaedic Translation, 2016. **5**: p. 9-15.
24. Remennik, S., et al., *New, fast corroding high ductility Mg–Bi–Ca and Mg–Bi–Si alloys, with no clinically observable gas formation in bone implants.* Materials Science and Engineering: B, 2011. **176**(20): p. 1653-1659.
25. Wu, G., J.M. Ibrahim, and P.K. Chu, *Surface design of biodegradable magnesium alloys—a review.* Surface and Coatings Technology, 2013. **233**: p. 2-12.
26. Dorozhkin, S.V., *Calcium orthophosphate coatings on magnesium and its biodegradable alloys.* Acta biomaterialia, 2014. **10**(7): p. 2919-2934.

27. Bamberger, M. and G. Dehm, *Trends in the development of new Mg alloys.* Annu. Rev. Mater. Res., 2008. **38**: p. 505-533.

28. Narayanan, T.S., I.-S. Park, and M.H. Lee, *Surface Modification of Magnesium and Its Alloys for Biomedical Applications: Modification and Coating Techniques.* Vol. 2. 2015: Elsevier.

29. Xin, Y., et al., *Corrosion behavior of biomedical AZ91 magnesium alloy in simulated body fluids.* Journal of materials research, 2007. **22**(07): p. 2004-2011.

30. Dziuba, D., et al., *Long-term in vivo degradation behaviour and biocompatibility of the magnesium alloy ZEK100 for use as a biodegradable bone implant.* Acta biomaterialia, 2013. **9**(10): p. 8548-8560.

31. Wu, Y., et al., *In vitro study on biodegradable AZ31 magnesium alloy fibers reinforced PLGA composite.* Journal of Materials Science & Technology, 2013. **29**(6): p. 545-550.

32. Liu, C., et al., *Influence of heat treatment on degradation behavior of bio-degradable die-cast AZ63 magnesium alloy in simulated body fluid.* Materials Science and Engineering: A, 2007. **456**(1): p. 350-357.

33. Zhang, X., et al., *Biocorrosion properties of as-extruded Mg–Nd–Zn–Zr alloy compared with commercial AZ31 and WE43 alloys.* Materials Letters, 2012. **66**(1): p. 209-211.

34. Wan, Y., et al., *Preparation and characterization of a new biomedical magnesium–calcium alloy.* Materials & Design, 2008. **29**(10): p. 2034-2037.

35. Li, Z., et al., *The development of binary Mg–Ca alloys for use as biodegradable materials within bone.* Biomaterials, 2008. **29**(10): p. 1329-1344.

36. Brar, H.S., J. Wong, and M.V. Manuel, *Investigation of the mechanical and degradation properties of Mg–Sr and Mg–Zn–Sr alloys for use as potential biodegradable implant materials.* Journal of the mechanical behavior of biomedical materials, 2012. **7**: p. 87-95.

37. Zhang, S., et al., *Research on an Mg–Zn alloy as a degradable biomaterial.* Acta Biomaterialia, 2010. **6**(2): p. 626-640.

38. Bakhsheshi-Rad, H., et al., *Mechanical and bio-corrosion properties of quaternary Mg–Ca–Mn–Zn alloys compared with binary Mg–Ca alloys.* Materials & Design, 2014. **53**: p. 283-292.

39. Rad, B., et al., *Characterization and corrosion behavior of biodegradable Mg-Ca and Mg-Ca-Zn implant alloys.* Applied Mechanics and Materials, 2012. **121**: p. 568-572.

40. Berglund, I.S., et al., *Synthesis and characterization of Mg-Ca-Sr alloys for biodegradable orthopedic implant applications.* Journal of Biomedical Materials Research Part B: Applied Biomaterials, 2012. **100**(6): p. 1524-1534.

41. Cha, P.-R., et al., *Biodegradability engineering of biodegradable Mg alloys: Tailoring the electrochemical properties and microstructure of constituent phases.* Scientific reports, 2013. **3**.

42. Sun, Y., et al., *Preparation and characterization of a new biomedical Mg–Zn–Ca alloy.* Materials & Design, 2012. **34**: p. 58-64.

43. Synthesis Companies. *Bone work from head to toe.* 2012 [cited 2015 15 Jan]; Available from: http://www.synthes.com/sites/NA/Products/Pages/default_home.aspx.

44. Gibson, I., D.W. Rosen, and B. Stucker, *Additive manufacturing technologies.* 2010: Springer.

45. Anitha, D., et al., *Improving stability of locking compression plates through a design modification: a computational investigation.* Computer methods in biomechanics and biomedical engineering, 2013(ahead-of-print): p. 1-9.

46. Raja Izaham, R.M.A., et al., *Finite element analysis of Puddu and Tomofix plate fixation for open wedge high tibial osteotomy.* Injury, 2012. **43**(6): p. 898-902.

47. Taheri, E., et al., *Effect of Screws Placement on Locking Compression Plate for Fixating Medial Transverse Fracture of Tibia.* Biomedical Engineering, 2012. **1**(1): p. 14-18.

48. Pal, S., et al. *Finite Element Analysis of Magnesium Alloy Based Bone Fixation Devices.* in *ASME 2013 Conference on Frontiers in Medical Devices: Applications of Computer Modeling and Simulation.* 2013. American Society of Mechanical Engineers.

49. Pietrzak, W.S., D. Sarver, and M. Verstynen, *Bioresorbable implants—practical considerations.* Bone, 1996. **19**(1): p. S109-S119.

50. Tsantrizos, A., et al., *Segmental stability and compressive strength of posterior lumbar interbody fusion implants.* Spine, 2000. **25**(15): p. 1899-1907.

51. Slowik, G. *Do metal plates and screws need to be removed from the bone after a fracture has healed?* 2013 [cited 2014 20 Jan]; Available from: http://ehealthmd.com/blog/should-metal-plates-and-screws-or-nail-hardware-be-removed-bone-now-my-fracture-has-healed#axzz3PQgYi5oR.

52. MIT. *Bone Plates/Materials.* 2001 [cited 2014 19 Jan]; Available from: http://web.mit.edu/3.082/www/team1s/background/materials.html.

53. Chiu, K., et al., *Characterization and corrosion studies of fluoride conversion coating on degradable Mg implants.* Surface and Coatings Technology, 2007. **202**(3): p. 590-598.

54. Suuronen, R., *Biodegradable fracture-fixation devices in maxillofacial surgery.* International journal of oral and maxillofacial surgery, 1993. **22**(1): p. 50-57.

55. Waris, E., et al., *Use of bioabsorbable osteofixation devices in the hand.* Journal of Hand Surgery (British and European Volume), 2004. **29**(6): p. 590-598.

56. Hermawan, H., *Biodegradable Metals: State of the Art*, in *Biodegradable Metals.* 2012, Springer. p. 13-22.

57. Ibrahim, H., et al., *Characteristics of starch-based biodegradable composites reinforced with date palm and flax fibers.* Carbohydrate polymers, 2014. **101**: p. 11-19.

58. Mehanny, S., et al. *Fabrication and Characterization of Starch Based Bagasse Fiber Composite*. in *ASME 2012 International Mechanical Engineering Congress and Exposition*. 2012. American Society of Mechanical Engineers.

59. Seitz, J.M., et al., *Magnesium degradation products: Effects on tissue and human metabolism.* Journal of Biomedical Materials Research Part A, 2014. **102**(10): p. 3744-3753.

60. Kirkland, N.T., et al., *Performance-driven design of Biocompatible Mg alloys.* JOM, 2011. **63**(6): p. 28-34.

61. Willbold, E., et al., *Effect of the addition of low rare earth elements (lanthanum, neodymium, cerium) on the biodegradation and biocompatibility of magnesium.* Acta biomaterialia, 2015. **11**: p. 554-562.

62. Hiromoto, S., et al., *In vitro and in vivo biocompatibility and corrosion behaviour of a bioabsorbable magnesium alloy coated with octacalcium phosphate and hydroxyapatite.* Acta biomaterialia, 2015. **11**: p. 520-530.

63. Witte, F., et al., *Implant made of a magnesium alloy and method for the production thereof.* 2014, Google Patents.

64. 2014 [cited 2016 25 May]; Available from: http://www.transluminal.net/news.html.

65. Lock, J.Y., et al., *Degradation and antibacterial properties of magnesium alloys in artificial urine for potential resorbable ureteral stent applications.* Journal of Biomedical Materials Research Part A, 2014. **102**(3): p. 781-792.

66. Campos, C.M., et al., *Bioresorbable drug-eluting magnesium-alloy scaffold for treatment of coronary artery disease.* International journal of molecular sciences, 2013. **14**(12): p. 24492-24500.

67. *New BIOTRONIK DREAMS Bioabsorbable Metal Drug Eluting Coronary Scaffold in First Patient*. 2013 [cited 2016 14 May]; Available from: http://www.medgadget.com/2013/10/biotronik-dreams.html.

68. 2015 [cited 2016 12 May]; Available from: http://www.aap.de/en/investors/news/2015/press-release-dated-21-january-2015.

69. [cited 2016 16 May]; Available from: http://www.syntellix.de/en/syntellix/.

70. Windhagen, H., et al., *Biodegradable magnesium-based screw clinically equivalent to titanium screw in hallux valgus surgery: short term results of the first prospective, randomized, controlled clinical pilot study.* BioMedical Engineering OnLine, 2013. **12**(1): p. 1-10.

71. Waizy, H., et al., *In vivo study of a biodegradable orthopedic screw (MgYREZr-alloy) in a rabbit model for up to 12 months.* J Biomater Appl, 2014. **28**(5): p. 667-75.

72. Castellani, C., et al., *Bone–implant interface strength and osseointegration: biodegradable magnesium alloy versus standard titanium control.* Acta Biomaterialia, 2011. **7**(1): p. 432-440.

73. Tan, L., et al., *Loss of mechanical properties in vivo and bone–implant interface strength of AZ31B magnesium alloy screws with Si-containing coating.* Acta biomaterialia, 2014. **10**(5): p. 2333-2340.

74. Chaya, A., et al., *Fracture healing using degradable magnesium fixation plates and screws.* Journal of Oral and Maxillofacial Surgery, 2015. **73**(2): p. 295-305.

75. Chaya, A., et al., *In vivo study of magnesium plate and screw degradation and bone fracture healing.* Acta biomaterialia, 2015. **18**: p. 262-269.

76. Diekmann, J., et al., *Examination of a biodegradable magnesium screw for the reconstruction of the anterior cruciate ligament: A pilot in vivo study in rabbits.* Materials Science and Engineering: C, 2015.

77. Nassiri, M., B. MacDonald, and J.M. O'Byrne, *Locking compression plate breakage and fracture non-union: a finite element study of three patient-specific cases.* European Journal of Orthopaedic Surgery & Traumatology, 2012. **22**(4): p. 275-281.

78. Bayraktar, H.H., et al., *Comparison of the elastic and yield properties of human femoral trabecular and cortical bone tissue.* Journal of biomechanics, 2004. **37**(1): p. 27-35.

79. Lee, J.-Y., et al., *Biomechanical Evaluation of Magnesium-Based Resorbable Metallic Screw System in a Bilateral Sagittal Split Ramus Osteotomy Model Using Three-Dimensional Finite Element Analysis.* Journal of Oral and Maxillofacial Surgery, 2014. **72**(2): p. 402. e1-402. e13.

80. Keenan, J., G. Chakrabarty, and J. Newman, *Treatment of supracondylar femoral fracture above total knee replacement by custom made hinged prosthesis.* The Knee, 2000. **7**(3): p. 165-170.

81. Harrysson, O.L., Y.A. Hosni, and J.F. Nayfeh, *Custom-designed orthopedic implants evaluated using finite element analysis of patient-specific computed tomography data: femoral-component case study.* BMC Musculoskeletal Disorders, 2007. **8**(1): p. 1.

82. Lethaus, B., et al., *Interval cranioplasty with patient-specific implants and autogenous bone grafts–Success and cost analysis.* Journal of Cranio-Maxillofacial Surgery, 2014. **42**(8): p. 1948-1951.

83. Kirkland, N., N. Birbilis, and M. Staiger, *Assessing the corrosion of biodegradable magnesium implants: a critical review of current methodologies and their limitations.* Acta biomaterialia, 2012. **8**(3): p. 925-936.

84. Witte, F., et al., *In vivo corrosion of four magnesium alloys and the associated bone response.* Biomaterials, 2005. **26**(17): p. 3557-3563.

85. Agha, N.A., et al., *Magnesium degradation influenced by buffering salts in concentrations typical of in vitro and in vivo models.* Materials Science and Engineering: C, 2016. **58**: p. 817-825.

86. Xin, Y., T. Hu, and P.K. Chu, *Influence of test solutions on in vitro studies of biomedical magnesium alloys.* Journal of The Electrochemical Society, 2010. **157**(7): p. C238-C243.

87. Gu, X., et al., *In vitro and in vivo studies on a Mg–Sr binary alloy system developed as a new kind of*

biodegradable metal. Acta Biomaterialia, 2012. **8**(6): p. 2360-2374.

88. Gu, X., et al., *In vitro corrosion and biocompatibility of binary magnesium alloys.* Biomaterials, 2009. **30**(4): p. 484-498.

89. Li, Y., et al., *Mg–Zr–Sr alloys as biodegradable implant materials.* Acta biomaterialia, 2012. **8**(8): p. 3177-3188.

90. Zhang, E., et al., *Microstructure, mechanical properties and bio-corrosion properties of Mg–Si (–Ca, Zn) alloy for biomedical application.* Acta biomaterialia, 2010. **6**(5): p. 1756-1762.

91. Witte, F., et al., *Degradable biomaterials based on magnesium corrosion.* Current Opinion in Solid State and Materials Science, 2008. **12**(5): p. 63-72.

92. Huanxin Wang, S.G., Yisheng Wang , Hongjian Liu, Haitao Wang , Liguo Wang, Chenxing Ren, Shijie Zhu, Kuisheng Chen, *In vivo degradation behavior of Ca-deficient hydroxyapatite coated Mg–Zn–Ca alloy for bone implant application.* Colloids and Surfaces B: Biointerfaces, 2011. **88**: p. 254– 259.

93. Wong, H.M., et al., *A biodegradable polymer-based coating to control the performance of magnesium alloy orthopaedic implants.* Biomaterials, 2010. **31**(8): p. 2084-2096.

94. Taljanovic, M.S., et al., *Fracture Fixation 1.* Radiographics, 2003. **23**(6): p. 1569-1590.

95. Erinc, M., et al. *Applicability of existing magnesium alloys as biomedical implant materials*. in *Magnesium Technology 2009, 15 February 2009 through 19 February 2009, San Francisco, CA, USA, Conference code: 76923, 209-214*. 2009.

96. Sankara Narayanan, T., I.S. Park, and M.H. Lee, *Strategies to improve the corrosion resistance of microarc oxidation (MAO) coated magnesium alloys for degradable implants: Prospects and challenges.* Progress in Materials Science, 2014. **60**: p. 1-71.

97. Song, G., *Control of biodegradation of biocompatable magnesium alloys.* Corrosion Science, 2007. **49**(4): p. 1696-1701.

98. Bornapour, M., et al., *Magnesium implant alloy with low levels of strontium and calcium: The third element effect and phase selection improve bio-corrosion resistance and mechanical performance.* Materials Science and Engineering: C, 2014. **35**: p. 267-282.

99. Saha, P., et al., *Effects of grain refinement on the biocorrosion and in vitro bioactivity of magnesium.* Materials Science and Engineering: C, 2015. **57**: p. 294-303.

100. Domingo, J.L., *Reproductive and developmental toxicity of aluminum: a review.* Neurotoxicology and teratology, 1995. **17**(4): p. 515-521.

101. Luckey, T. and B. Venugopal, *Metal toxicity in mammals. Volume 1: Physiologic and chemical basis for metal toxicity.* Metal toxicity in mammals. Volume 1. Physiologic and chemical basis for metal toxicity., 1977.

102. Flaten, T.P., *Aluminium as a risk factor in Alzheimer's disease, with emphasis on drinking water.* Brain research bulletin, 2001. **55**(2): p. 187-196.

103. CASES, N., *Macrophagic myofasciitis associated with vaccine-derived aluminium.* The Medical Journal of Australia, 2005. **183**(3): p. 145-146.

104. Bruce, D.W., B.E. Hietbrink, and K.P. DuBois, *The acute mammalian toxicity of rare earth nitrates and oxides.* Toxicology and applied pharmacology, 1963. **5**(6): p. 750-759.

105. Hirano, S., et al., *Metabolism and toxicity of intravenously injected yttrium chloride in rats.* Toxicology and applied pharmacology, 1993. **121**(2): p. 224-232.

106. Lee, J.-Y., et al., *Effects of impurities on the biodegradation behavior of pure magnesium.* Metals and Materials International, 2009. **15**(6): p. 955-961.

107. Poinern, G.E.J., S. Brundavanam, and D. Fawcett, *Biomedical magnesium alloys: a review of material properties, surface modifications and potential as a biodegradable orthopaedic implant.* American Journal of Biomedical Engineering, 2012. **2**(6): p. 218-240.

108. Shih, T.-S., J.-H. Wang, and K.-Z. Chong, *Combustion of magnesium alloys in air.* Materials Chemistry and Physics, 2004. **85**(2): p. 302-309.

109. Mezbahul-Islam, M., A.O. Mostafa, and M. Medraj, *Essential magnesium alloys binary phase diagrams and their thermochemical data.* Journal of Materials, 2014. **2014**.

110. Aljarrah, M. and M. Medraj, *Thermodynamic modelling of the Mg–Ca, Mg–Sr, Ca–Sr and Mg–Ca–Sr systems using the modified quasichemical model.* Calphad, 2008. **32**(2): p. 240-251.

111. Nayeb-Hashemi, A. and J. Clark, *The Ca− Mg (Calcium-Magnesium) system.* Journal of Phase Equilibria, 1987. **8**(1): p. 58-65.

112. Ghosh, P., M. Mezbahul-Islam, and M. Medraj, *Critical assessment and thermodynamic modeling of Mg–zn, Mg–sn, Sn–Zn and Mg–Sn–Zn systems.* Calphad, 2012. **36**: p. 28-43.

113. Koç, E., et al., *Influence of zinc on the microstructure, mechanical properties and in vitro corrosion behavior of magnesium–zinc binary alloys.* Journal of Alloys and Compounds, 2015. **648**: p. 291-296.

114. Vojtěch, D., et al., *Mechanical and corrosion properties of newly developed biodegradable Zn-based alloys for bone fixation.* Acta biomaterialia, 2011. **7**(9): p. 3515-3522.

115. Murni, N., et al., *Cytotoxicity evaluation of biodegradable Zn–3Mg alloy toward normal human osteoblast cells.* Materials Science and Engineering: C, 2015.

116. Liu, X., et al., *Micro-alloying with Mn in Zn–Mg alloy for future biodegradable metals application.* Materials & Design, 2016. **94**: p. 95-104.

117. Song, Y., D. Shan, and E.-H. Han, *A novel biodegradable nicotinic acid/calcium phosphate composite coating on Mg–3Zn alloy.* Materials Science and Engineering: C, 2013. **33**(1): p. 78-84.

118. Zhao, Y., et al., *High strength Mg–Zn–Ca alloys prepared by atomization and hot pressing process.* Materials Letters, 2014. **118**: p. 55-58.

119. Farahany, S., et al., *In-situ thermal analysis and macroscopical characterization of Mg–xCa and Mg–0.5 Ca–xZn alloy systems.* Thermochimica Acta, 2012. **527**: p. 180-189.

120. Bakhsheshi-Rad, H., et al., *Relationship between the corrosion behavior and the thermal characteristics and microstructure of Mg–0.5 Ca–xZn alloys.* Corrosion Science, 2012. **64**: p. 184-197.

121. Zhang, E. and L. Yang, *Microstructure, mechanical properties and bio-corrosion properties of Mg–Zn–Mn–Ca alloy for biomedical application.* Materials Science and Engineering: A, 2008. **497**(1): p. 111-118.

122. Larionova, T.V., W.-W. Park, and B.-S. You, *A ternary phase observed in rapidly solidified Mg–Ca–Zn alloys.* Scripta Materialia, 2001. **45**(1): p. 7-12.

123. Jardim, P.M., G. Solórzano, and J.B.V. Sande, *Precipitate crystal structure determination in melt spun Mg-1.5 wt% Ca-6wt% Zn alloy.* Microscopy and Microanalysis, 2002. **8**(06): p. 487-496.

124. Zander, D. and N.A. Zumdick, *Influence of Ca and Zn on the microstructure and corrosion of biodegradable Mg–Ca–Zn alloys.* Corrosion Science, 2015. **93**: p. 222-233.

125. Du, H., et al., *Effects of Zn on the microstructure, mechanical property and bio-corrosion property of Mg–3Ca alloys for biomedical application.* Materials Chemistry and Physics, 2011. **125**(3): p. 568-575.

126. Rad, B., et al. *Characterization and corrosion behavior of biodegradable Mg-Ca and Mg-Ca-Zn implant alloys.* in *Applied Mechanics and Materials.* 2012. Trans Tech Publ.

127. Gu, X., et al., *Corrosion of, and cellular responses to Mg–Zn–Ca bulk metallic glasses.* Biomaterials, 2010. **31**(6): p. 1093-1103.

128. Zberg, B., P.J. Uggowitzer, and J.F. Löffler, *MgZnCa glasses without clinically observable hydrogen evolution for biodegradable implants.* Nature Materials, 2009. **8**(11): p. 887-891.

129. Cao, J., et al., *Ca–Mg–Zn bulk metallic glasses as bioresorbable metals.* Acta biomaterialia, 2012. **8**(6): p. 2375-2383.

130. Gu, X., et al., *Mg–Ca–Zn bulk metallic glasses with high strength and significant ductility.* Journal of materials research, 2005. **20**(08): p. 1935-1938.

131. Zhang, E., et al., *Microstructure, mechanical and corrosion properties and biocompatibility of Mg–Zn–Mn alloys for biomedical application.* Materials Science and Engineering: C, 2009. **29**(3): p. 987-993.

132. Qu, Y., et al., *Evaluation of a new Mg–Zn–Ca–Y alloy for biomedical application.* Journal of Materials Science: Materials in Medicine, 2015. **26**(1): p. 1-7.

133. Shadanbaz, S. and G.J. Dias, *Calcium phosphate coatings on magnesium alloys for biomedical applications: a review.* Acta Biomaterialia, 2012. **8**(1): p. 20-30.

134. Krishna, L.R. and G. Sundararajan, *Aqueous corrosion behavior of micro arc oxidation (MAO)-coated magnesium alloys: a critical review.* JOM, 2014. **66**(6): p. 1045-1060.

135. X.N. Gu, W.Z., Y. Cheng, Y.F. Zheng, *A study on alkaline heat treated Mg–Ca alloy for the control of the biocorrosion rate.* Acta Biomaterialia, 2009. **5**: p. 2790–2799.

136. Ting Lei, C.O., Wei Tang, Lian-Feng Li, Le-Shan Zhou, *Enhanced corrosion protection of MgO coatings on magnesium alloy deposited by an anodic electrodeposition process.* Corrosion Science, 2010. **52**: p. 3504–3508.

137. Mousa, H.M., et al., *A novel Simple Strategy for in situ Deposition of Apatite layer on AZ31B Magnesium alloy for Bone Tissue Regeneration.* Applied Surface Science, 2015.

138. Malayoglu, U., K.C. Tekin, and S. Shrestha, *Influence of post-treatment on the corrosion resistance of PEO coated AM50B and AM60B Mg alloys.* Surface and Coatings Technology, 2010. **205**(6): p. 1793-1798.

139. Arrabal, R., et al., *Assessment of duplex coating combining plasma electrolytic oxidation and polymer layer on AZ31 magnesium alloy.* Surface and Coatings Technology, 2012. **206**(22): p. 4692-4703.

140. Gray, J. and B. Luan, *Protective coatings on magnesium and its alloys—a critical review.* Journal of alloys and compounds, 2002. **336**(1): p. 88-113.

141. Guo, H. and M. An, *Growth of ceramic coatings on AZ91D magnesium alloys by micro-arc oxidation in aluminate–fluoride solutions and evaluation of corrosion resistance.* Applied Surface Science, 2005. **246**(1): p. 229-238.

142. Wang, Y.-M., et al., *Biocorrosion resistance of coated magnesium alloy by microarc oxidation in electrolyte containing zirconium and calcium salts.* Frontiers of Materials Science, 2014. **8**(3): p. 295-306.

143. Liu, J., et al., *Effect of microarc oxidation time on electrochemical behaviors of coated bio-compatible magnesium alloy.* Materials Today: Proceedings, 2014. **1**(1): p. 70-81.

144. Lin, X., et al., *Effect of preparation parameters on the properties of hydroxyapatite containing micro-arc oxidation coating on biodegradable ZK60 magnesium alloy.* Ceramics International, 2014. **40**(7): p. 10043-10051.

145. Narayanan, T.S., I.S. Park, and M.H. Lee, *Strategies to improve the corrosion resistance of microarc oxidation (MAO) coated magnesium alloys for degradable implants: Prospects and challenges.* Progress in Materials Science, 2014. **60**: p. 1-71.

146. Guo, M., et al., *Anticorrosion and cytocompatibility behavior of MAO/PLLA modified magnesium alloy WE42.* Journal of Materials Science: Materials in Medicine, 2011. **22**(7): p. 1735-1740.

34

147. Cai, J., et al., *The preparation and corrosion behaviors of MAO coating on AZ91D with rare earth conversion precursor film.* Applied Surface Science, 2011. **257**(8): p. 3804-3811.

148. Mu, W. and Y. Han, *Characterization and properties of the MgF 2/ZrO 2 composite coatings on magnesium prepared by micro-arc oxidation.* Surface and Coatings Technology, 2008. **202**(17): p. 4278-4284.

149. Wang, H., et al., *In vitro degradation and mechanical integrity of Mg–Zn–Ca alloy coated with Ca-deficient hydroxyapatite by the pulse electrodeposition process.* Acta Biomaterialia, 2010. **6**(5): p. 1743-1748.

150. Niu, J., et al., *Enhanced biocorrosion resistance and biocompatibility of degradable Mg–Nd–Zn–Zr alloy by brushite coating.* Materials Science and Engineering: C, 2013. **33**(8): p. 4833-4841.

151. Guan, X., et al., *Enhancement of osteogenesis and biodegradation control by brushite coating on Mg–Nd–Zn–Zr alloy for mandibular bone repair.* ACS applied materials & interfaces, 2014. **6**(23): p. 21525-21533.

152. Zhao, L., et al., *Corrosion resistance and calcium–phosphorus precipitation of micro-arc oxidized magnesium for biomedical applications.* Applied Surface Science, 2015. **330**: p. 431-438.

153. Dou, J., et al., *Formation of calcium phosphate coating on Mg-Zn-Ca alloy by micro-arc oxidation technique.* Materials Letters, 2016. **164**: p. 575-578.

154. Li, J., et al., *In vitro degradation and cell attachment of a PLGA coated biodegradable Mg–6Zn based alloy.* Journal of Materials Science, 2010. **45**(22): p. 6038-6045.

155. Xu, L. and A. Yamamoto, *Characteristics and cytocompatibility of biodegradable polymer film on magnesium by spin coating.* Colloids and Surfaces B: Biointerfaces, 2012. **93**: p. 67-74.

156. Wong, H.M., et al., *A biodegradable polymer-based coating to control the performance of magnesium alloy orthopaedic implants.* Biomaterials, 2010. **31**(8): p. 2084-2096.

157. Li, L.-H., et al., *Deposition of microarc oxidation–polycaprolactone duplex coating to improve the corrosion resistance of magnesium for biodegradable implants.* Thin Solid Films, 2014. **562**: p. 561-567.

158. Zomorodian, A., et al., *"In-vitro" corrosion behaviour of the magnesium alloy with Al and Zn (AZ31) protected with a biodegradable polycaprolactone coating loaded with hydroxyapatite and cephalexin.* Electrochimica Acta, 2015.

159. Zhao, S., et al., *A dual-task design of corrosion-controlling and osteo-compatible hexamethylenediaminetetrakis-(methylene phosphonic acid)(HDTMPA) coating on magnesium for biodegradable bone implants application.* Journal of Biomedical Materials Research Part A, 2015. **103**(5): p. 1640-1652.

160. Razavi, M., et al., *Controlling the degradation rate of bioactive magnesium implants by electrophoretic deposition of akermanite coating.* Ceramics International, 2014. **40**(3): p. 3865-3872.

161. Zhao, Y., et al., *Enhanced antimicrobial properties, cytocompatibility, and corrosion resistance of plasma-modified biodegradable magnesium alloys.* Acta biomaterialia, 2014. **10**(1): p. 544-556.

162. Yan, T., et al., *Fluoride Conversion Coating on Biodegradable AZ31B Magnesium Alloy.* Journal of Materials Science & Technology, 2014. **30**(7): p. 666-674.

163. Razavi, M., et al., *In vitro study of nanostructured diopside coating on Mg alloy orthopedic implants.* Materials Science and Engineering: C, 2014. **41**: p. 168-177.

164. Zomorodian, A., et al., *Biofunctional composite coating architectures based on polycaprolactone and nanohydroxyapatite for controlled corrosion activity and enhanced biocompatibility of magnesium AZ31 alloy.* Materials Science and Engineering: C, 2015. **48**: p. 434-443.

165. Sanchez, A.H.M., et al., *Mg and Mg alloys: How comparable are in vitro and in vivo corrosion rates? A review.* Acta biomaterialia, 2015. **13**: p. 16-31.

166. Gu, Y., et al., *Corrosion mechanism and model of pulsed DC microarc oxidation treated AZ31 alloy in simulated body fluid.* Applied Surface Science, 2012. **258**(16): p. 6116-6126.

167. Wang, H., et al., *In vivo degradation behavior of Ca-deficient hydroxyapatite coated Mg–Zn–Ca alloy for bone implant application.* Colloids and Surfaces B: Biointerfaces, 2011. **88**(1): p. 254-259.

168. Kainer, K.U. and F. Kaiser, *Magnesium alloys and technology.* 2003.

169. Mordike, B. and T. Ebert, *Magnesium: Properties—applications—potential.* Materials Science and Engineering: A, 2001. **302**(1): p. 37-45.

170. Luo, A.A., *Magnesium casting technology for structural applications.* Journal of Magnesium and Alloys, 2013. **1**(1): p. 2-22.

171. Gupta, M. and G.K. Meenashisundaram, *Synthesis of Magnesium-Based Biomaterials*, in *Insight into Designing Biocompatible Magnesium Alloys and Composites*. 2015, Springer. p. 17-34.

172. Wang, H., Y. Estrin, and Z. Zúberová, *Bio-corrosion of a magnesium alloy with different processing histories.* Materials Letters, 2008. **62**(16): p. 2476-2479.

173. Walde, T. and H. Riedel, *Modeling texture evolution during hot rolling of magnesium alloy AZ31.* Materials Science and Engineering: A, 2007. **443**(1): p. 277-284.

174. Wagner, L., *Mechanical surface treatments on titanium, aluminum and magnesium alloys.* Materials Science and Engineering: A, 1999. **263**(2): p. 210-216.

175. Birbilis, N. and Y. Estrin, *Corrosion of pure Mg as a function of grain size and processing route.* Advanced Engineering Materials, 2008. **10**(6): p. 579-582.

176. Avedesian, M.M. and H. Baker, *ASM specialty handbook: magnesium and magnesium alloys.* ASM International, Materials Park, OH, 1999: p. 15.

177. Nie, J. and B. Muddle, *Precipitation hardening of Mg-Ca (-Zn) alloys.* Scripta Materialia, 1997. **37**(10): p. 1475-1481.

178. Yue, T., L. Yan, and H. Man, *The Effect of Machined Surface Condition on the Corrosion Behavior of Magnesium ZM51/SiC Composite.* Materials and Manufacturing Processes, 2004. **19**(2): p. 123-138.

179. Fu, P., et al., *Low-pressure die casting of magnesium alloy AM50: Response to process parameters.* journal of materials processing technology, 2008. **205**(1): p. 224-234.

180. Zhiqiang, S.H.Z.M.G., *Overview and Prospect of Semi Solid Casting [J].* Special Casting & Nonferrous Alloys, 1998. **5**.

181. Ghomashchi, M. and A. Vikhrov, *Squeeze casting: an overview.* Journal of Materials Processing Technology, 2000. **101**(1): p. 1-9.

182. Luo, A., et al., *Magnesium castings for automotive applications.* Jom, 1995. **47**(7): p. 28-31.

183. Luo, A. and M. Pekguleryuz, *Cast magnesium alloys for elevated temperature applications.* Journal of Materials Science, 1994. **29**(20): p. 5259-5271.

184. Inoue, A., et al., *Mg–Cu–Y bulk amorphous alloys with high tensile strength produced by a high-pressure die casting method.* Materials Transactions, JIM, 1992. **33**(10): p. 937-945.

185. Vinarcik, E.J., *High integrity die casting processes.* 2002: John Wiley & Sons.

186. Aghion, E. and B. Bronfin. *Magnesium alloys development towards the 21st century.* in *Materials Science Forum.* 2000. Trans Tech Publ.

187. Brown, Z., et al., *Development of super-vacuum die casting process for magnesium alloys.* North American Die Casting Association Transactions, T09-043, 2009: p. 723-729.

188. Patel, H., et al., *Cyclic deformation behavior of a super-vacuum die cast magnesium alloy.* Materials Science and Engineering: A, 2012. **546**: p. 72-81.

189. Nehan, M. and R. Maloney, *Magnesium AM60B instrument panel structure for crashworthiness FMVSS 204 and 208 compliance.* 1996, SAE Technical Paper.

190. Avedesian, M. and H. Baker, *Magnesium and magnesium alloys.* 1998.

191. Luo, A.A., A.K. Sachdev, and B.R. Powell, *Advanced casting technologies for lightweight automotive applications.* China Foundry, 2010. **7**(4): p. 463-469.

192. Gutman, E., et al., *Influence of technological parameters of permanent mold casting and die casting on creep and strength of Mg alloy AZ91D.* Materials Science and Engineering: A, 1997. **234**: p. 880-883.

193. Dahle, A.K., et al., *Development of the as-cast microstructure in magnesium–aluminium alloys.* Journal of light metals, 2001. **1**(1): p. 61-72.

194. Hsiang, S.-H. and J.-L. Kuo, *An investigation on the hot extrusion process of magnesium alloy sheet.* Journal of Materials Processing Technology, 2003. **140**(1): p. 6-12.

195. Li, J., et al., *Study on microstructure and properties of extruded Mg–2Nd–0.2 Zn alloy as potential biodegradable implant material.* Materials Science and Engineering: C, 2015. **49**: p. 422-429.

196. Denkena, B. and A. Lucas, *Biocompatible magnesium alloys as absorbable implant materials–adjusted surface and subsurface properties by machining processes.* CIRP Annals-Manufacturing Technology, 2007. **56**(1): p. 113-116.

197. Sunil, B.R., et al., *In vitro and in vivo studies of biodegradable fine grained AZ31 magnesium alloy produced by equal channel angular pressing.* Materials Science and Engineering: C, 2016. **59**: p. 356-367.

198. Zhang, C., et al., *Microstructures and degradation mechanism in simulated body fluid of biomedical Mg–Zn–Ca alloy processed by high pressure torsion.* Materials & Design, 2016. **96**: p. 54-62.

199. Jayaraj, J., et al., *Enhanced precipitation hardening of Mg–Ca alloy by Al addition.* Scripta Materialia, 2010. **63**(8): p. 831-834.

200. Sun, X., et al., *Mechanical and corrosion properties of newly developed Mg-Mn-Ca alloys as potential biodegradable implant materials.* Corrosion Engineering, Science and Technology, 2014. **49**(4): p. 303-310.

201. Zeng, R., et al., *Progress and challenge for magnesium alloys as biomaterials.* Advanced Engineering Materials, 2008. **10**(8): p. B3-B14.

202. Gladman, T., *Precipitation hardening in metals.* Materials Science and Technology, 1999. **15**(1): p. 30-36.

203. Gao, X., et al., *Precipitation-hardened Mg–Ca–Zn alloys with superior creep resistance.* Scripta materialia, 2005. **53**(12): p. 1321-1326.

204. Bettles, C., M. Gibson, and K. Venkatesan, *Enhanced age-hardening behaviour in Mg–4 wt.% Zn micro-alloyed with Ca.* Scripta Materialia, 2004. **51**(3): p. 193-197.

205. Oh, J., et al., *TEM and 3DAP characterization of an age-hardened Mg–Ca–Zn alloy.* Scripta materialia, 2005. **53**(6): p. 675-679.

206. Lu, Y., et al., *Effects of secondary phase and grain size on the corrosion of biodegradable Mg–Zn–Ca alloys.* Materials Science and Engineering: C, 2015. **48**: p. 480-486.

207. Höh, N.V.D., et al., *Influence of Different Surface Machining Treatments of Magnesium-based Resorbable Implants on the Degradation Behavior in Rabbits.* Advanced Engineering Materials, 2009. **11**(5): p. B47-B54.

208. Polmear, I., *Magnesium alloys and applications.* Materials science and technology, 1994. **10**(1): p. 1-16.

209. Ng, C., et al., *Layer manufacturing of magnesium and its alloy structures for future applications.* Virtual and Physical Prototyping, 2010. **5**(1): p. 13-19.

210. Bremen, S., W. Meiners, and A. Diatlov, *Selective Laser Melting.* Laser Technik Journal, 2012. **9**(2): p. 33-38.

211. Chung Ng, C., M. Savalani, and H. Chung Man, *Fabrication of magnesium using selective laser melting technique.* Rapid Prototyping Journal, 2011. **17**(6): p. 479-490.

212. Ng, C., et al., *Microstructure and mechanical properties of selective laser melted magnesium.* Applied Surface Science, 2011. **257**(17): p. 7447-7454.

213. Savalani, M.M., et al., *Effect of preheat and layer thickness on selective laser melting (SLM) of magnesium.* Rapid Prototyping Journal, 2016. **22**(1).

214. Matena, J., et al., *Comparison of selective laser melted titanium and magnesium implants coated with PCL.* International journal of molecular sciences, 2015. **16**(6): p. 13287-13301.

215. Holland, L., *Vacuum manual*. 2012: Springer Science & Business Media.

216. Leong, K., *Laser beam welding of any metal*. 1998, Argonne National Lab., IL (US).

217. Nölke, C., *A cure in 3D*, in *The Trumpf Laser Magazine*. 2013, Laser-Community: Hannover, Germany. p. 5.

218. Zhang, B., H. Liao, and C. Coddet, *Effects of processing parameters on properties of selective laser melting Mg–9% Al powder mixture.* Materials & Design, 2012. **34**: p. 753-758.

219. Giesekel, M., et al., *Selective Laser Melting of Magnesium and Magnesium Alloys.* Magnesium Technology 2013, 2013: p. 65-68.

220. Askeland, D.R. and P.P. Phulé, *The science and engineering of materials.* 2003.

221. Fraunhofer Institute for Laser Technology ILT. *Selective laser melting of magnesium alloys*. 2014 [cited 2014 16 Dec]; Available from: http://www.ilt.fraunhofer.de/en/publication-and-press/annual-report/2012/annual-report-2012-p88.html.

222. Roland, L., et al., *Poly-ε-caprolactone Coated and Functionalized Porous Titanium and Magnesium Implants for Enhancing Angiogenesis in Critically Sized Bone Defects.* International journal of molecular sciences, 2015. **17**(1): p. 1.

223. Tech Briefs. *$19 Million Funding Awarded for Additive Manufacturing Projects*. 2014 [cited 2014 3 Nov]; Available from: http://www.techbriefs.com/component/content/article/10-ntb/tech-briefs/bio-medical/19171.

224. Halterman, T. *Biodegradable 3d Printed Metal Bone Scaffolding*. 2014 [cited 2015 2 July]; Available from: http://www.3dprinterworld.com/article/biodegradable-3d-printed-metal-bone-scaffolding.